



# 1 The new TSMP2 coupled Earth system model

3 Stefan Poll<sup>1,2,3</sup>, Paul Rigor<sup>2,3</sup>, Slavko Brdar<sup>4</sup>, Ha Thi Minh Ho-Hagemann<sup>5</sup>, Carl Hartick<sup>6</sup>, Marco van Hulten<sup>7</sup>, Ana 4 Gonzalez-Nicolas<sup>2,3</sup>, Johannes Keller<sup>1,3</sup>, Daniel Caviedes-Voullieme<sup>1,2,3</sup>, Harrie-Jan Hendricks-Franssen<sup>1,3</sup>, Klaus Goergen<sup>1,3</sup>, 5 Stefan Kollet<sup>1,3</sup> 7 <sup>1</sup> Institute for Bio- and Geosciences (Agrosphere, IBG-3), Research Centre Jülich, Jülich, Germany 8 <sup>2</sup> CASA Simulation and Data Laboratory Terrestrial Systems, Jülich Supercomputing Centre (JSC), Jülich, Germany 9 <sup>3</sup> Centre for High-Performance Scientific Computing in Terrestrial Systems, Geoverbund ABC/J, Jülich, Germany 10 <sup>4</sup> European Centre for Medium-Range Weather Forecasts, Reading, UK 11 <sup>5</sup> Institute of Coastal Research, Helmholtz-Zentrum Hereon, Geesthacht, Germany 12 <sup>6</sup> Deutscher Wetterdienst, Offenbach, Germany 13 <sup>7</sup> High Performance Computing and Analytics Lab, University of Bonn, Bonn, Germany 14 15 Correspondence to: Stefan Poll (s.poll@fz-juelich.de) 16 17 18 19 Abstract. The Terrestrial Systems Modeling Platform (TSMP, github.com/HPSCTerrSys/TSMP2) is a scale-consistent, 20 highly modular, physics-based, massively parallel, and fully integrated coupled groundwater-vegetation-atmosphere 21 modeling system for regional Earth system modeling. TSMP is composed of the atmospheric models ICON or COSMO, the 22 land surface model Community Land Model (CLM), and the ParFlow subsurface-surface hydrological model, linked to 23 each other through the OASIS3-MCT coupler. TSMP is used across a wide range of spatio-temporal scales, ranging from 24 individual field plots, large eddy simulations to continental scale climate mode runs in a variety of applied research topics, 25 such as water resources, land-atmosphere coupling, or climate change projections. In version 2, or short TSMP2, we have 26 comprehensively modernized the coupled model system. One of the main changes from version 1 is the replacement of 27 component models with their current state-of-the-art successors for the atmosphere and the land surface, and a modified 28 coupling design to improve the mass and energy balances between the compartments. TSMP2 now relies entirely on a 29 CMake build-system, which enhances the system's portability across different computer infrastructures. Through a 30 Git-based framework TSMP2 includes auxiliary tools for model setup, a workflow engine and case study simulation 31 experiments to meet reproducibility, research software engineering, and FAIR data best practices. The TSMP2 coupled 32 model system and all its components are free open-source software. Aside from a description of the TSMP2 infrastructure, 33 we present the impact of coupling approaches between the compartments on model states in TSMP2, and outline our 34 development strategy along with technical and performance aspects arising from the coupling.





## 35 1. Introduction

36 This model description paper presents version 2.0 of the Terrestrial Systems Modelling Platform (hereafter TSMP2), a 37 regional earth system model (RESM) with a focus on terrestrial hydrology. The TSMP2 is the next-generation 38 reimplementation of the TSMP1 software platform and concept, first introduced by Shrestha et al. (2014).

39

40 With an intensifying water cycle and an increase in (projected) hydrometeorological extremes, such as heavy precipitation 41 or droughts, accurately representing and closing the coupled terrestrial water and energy cycles is vital for understanding the 42 climate system (Huntington, 2006; Mbabazi et al., 2025; Trenberth, 2011). Many relevant feedback processes, such as soil 43 moisture temperature or soil moisture precipitation feedback loops, are linked to and influenced by mass, energy and 44 momentum transfers between the subsurface, including groundwater, land surface, vegetation, and atmosphere, across a 45 wide range of spatial and temporal scales (Heinze et al., 2019). The interactions between these compartments play a critical 46 role in regulating the Earth's climate (Avissar and Pielke, 1989) and need to be explicitly simulated to improve predictions 47 of climate variability, water resources availability, and ecosystem responses under changing environmental conditions. 48 Despite this complexity, regional climate models (RCMs) often have a simplified representation of hydrological processes, 49 where only a 1D vertical subsurface water flow and free drainage at the lower boundary are combined with runoff 50 generation at the land surface without a lateral redistribution of surface and subsurface water. A simplified representation 51 leads to a resolution-dependent impact on flux partitioning at the land surface, land-atmosphere coupling, and affects the 52 land water balance and hydrometeorology (e.g. Barlage et al., 2021; Poshyvailo-Strube et al., 2024). To overcome these 53 limitations, the TSMP was developed as a coupled regional climate system model applicable across a wide range of scales 54 and for various purposes (from weather forecasting to climate change projections) enabling a physically consistent 55 simulation of the hydrological cycle and terrestrial system feedbacks (Shrestha et al., 2014).

56

57 Aside from TSMP, recent years have seen a number of developments that aim to improve model structure, towards a more 58 realistic process representation, and uses of coupled regional Earth system models. Examples for RESMs with a coupled 59 ocean and simulation of river include the CNRM-RCSM4 over the Mediterranean (Sevault et al., 2014), the recent 60 implementation of the ICON-CLM atmospheric model coupled to the GCOST-AHOI ocean, and the HD hydrological 61 discharge model by Ho-Hagemann et al. (2024) with a similar coupling approach as used in TSMP2 for the North Sea and 62 the Baltic. Primo et al. (2019) use COSMO RCM coupled to different versions of NEMO, covering all European marginal 63 seas. With respect to terrestrial hydrology, the WRF-Hydro (Lahmers et al., 2019) is a widespread model system that can 64 simulate overland flow and river discharge, but does not explicitly simulate 3D groundwater flow. Recent applications of 65 WRF-Hydro include Arnault et al. (2025), who investigate the sensitivity to soil hydraulic properties, or Zhang et al. (2025), 66 who showed that a lake-reservoir improved the simulation of streamflow. The groundwater capability was added with 67 WRF-ParFlow coupling by Williams III et al. (2013). The lateral subsurface flow alters the flux partitioning in a landscape 68 between convergence zones in river valleys and ridges. To account for it, less code-intrusive and computationally more 69 efficient approaches that modify the groundwater parametrization in existing land surface models (LSM) also exist. Barlage 70 et al. (2021) use the 3D groundwater scheme of Miguez-Macho et al. (2007) within the Noah-MP LSM to reduce the warm 71 bias in WRF continental US simulations, and to demonstrate an increased impact of groundwater on hydroclimate going 72 towards convection-permitting km-scale simulations. Schlemmer et al. (2018) implemented a topography-driven 73 groundwater runoff formulation into the TERRA LSM in the COSMO RCM that also reduces air temperature biases. The





74 RCSM modeling approaches are meanwhile mature enough to be included as so-called increased complexity models in the 75 current Coordinated Regional Downscaling Experiment (CORDEX) dynamical downscaling regional climate change 76 ensemble (Katragkou et al., 2024).

77

78 The TSMP version 1 (TSMP1, previously also abbreviated as TerrSysMP) was developed by Shrestha et al. (2014) with 79 later-on performance improvements by Gasper et al. (2014). TSMP is a fully integrated, physics-based 80 soil-vegetation-atmosphere RCSM where an atmospheric model, a land surface model, and an integrated hydrologic model 81 are linked with each other through an external coupler for flux exchange along compartmental interfaces - the land surface, 82 following the same coupling paradigm as most RCSMs from above, as opposed to process-based coupling (e.g., Jöckel et 83 al., 2010). An outstanding feature of TSMP is the incorporation of hydrologic processes through 3D soil and groundwater 84 hydrodynamics, solved in a continuum approach with 2D overland flow, linking groundwater with atmospheric processes 85 through the land surface. Hence, TSMP enables physically consistent, two-way exchanges of water, energy, and carbon in 86 the terrestrial system. This combination of an atmospheric, land surface and hydrological model allows for a more holistic 87 understanding of terrestrial feedbacks and interactions, such as how precipitation is partitioned into evapotranspiration and 8 runoff, how soil moisture dynamics affect atmospheric boundary layers, or how groundwater-surface water interactions 90 influence land-climate feedbacks. Such model systems help to integrate traditionally separate modelling realms into a 90 coherent terrestrial system perspective (Fersch et al., 2020).

91

92 The TSMP1 concept's usefulness and applicability have been shown in several studies. TSMP1 has been run temporally and 93 spatially from local domains over a few hours (Zhang et al., 2023) to regional domains over several years (Sulis et al., 2010) 94 to climate projections on a pan-European scale (Furusho-Percot et al., 2019) and for short- to medium-range weather 95 forecasts (Kollet et al., 2018). The modelling system was also used to show the relationship between the groundwater 96 representation and the evolution of hydrometeorological extremes, such as the August 2003 European heat wave (Keune et 97 al., 2016). With its groundwater-to-atmosphere feedbacks, TSMP can reproduce heatwave statistics in CORDEX ERA5 98 driven evaluation runs (Furusho-Percot et al., 2019) in comparison to RCMs with a more simplified hydrology 99 representation more accurately (Furusho-Percot et al., 2022). In a water resources study (Hartick et al., 2021) could show 100 the effect of groundwater dynamics on the long-term persistence of subsurface water storage anomalies. Keune et al. (2018) 101 investigated human interventions with the water cycle and water resources by groundwater abstraction and irrigation. Zipper 102 et al. (2019) studied the effect of remote land-atmosphere feedbacks due to land use and land cover change that lead to 103 widespread changes of energy and water balances, e.g., through substantial increases in cloud cover, while shallow 104 groundwater mitigates those heterogeneous impacts. Similarly, Hartick et al. (2022) described a feedback loop based on a 105 coupled TSMP1 evaluation simulation, where groundwater droughts systematically increase net solar incoming radiation 106 through a cloud feedback mechanism, which amplifies the drought. Using a new diagnostic, Zhang et al. (2024) analyse the 107 relationship between evapotranspiration and cloud water dynamics, which can spatially be associated with water- and 108 energy-limited coupling regimes.

109

110 Although TSMP1 has proven its versatility in these studies, there are some technical shortcomings, which led to the TSMP2 111 development. TSMP1 uses the COSMO v5.01 (COnsortium for Small-scale MOdeling; Baldauf et al., 2011) atmospheric 112 model and the CLM v3.5 (Community Land Model; Oleson et al., 2004). Both of these component models are no longer





113 updated and receive increasingly less community support. New features, such as transient aerosols, or greenhouse gas 114 concentration pathways for COSMO need to be backported. Parallel I/O, necessary for large, km-scale model domains, is 115 not available. The CLM3.5 land surface model does not offer dynamic vegetation, and features only a simplified urban 116 representation, which is also highly relevant for km-scale simulations. Additionally, the coupling of CLM3.5 was limited to 117 vegetation landunits.

118

119 TSMP2 builds on the foundations of TSMP1 and past experience and constitutes a comprehensive redesign of the model 120 system. With TSMP2, the model system has been significantly updated, offering enhanced capabilities for simulating and 121 analyzing interactions within terrestrial systems, including human interventions, dynamic vegetation, biogeochemical 122 cycles, or urban areas. TSMP2 has all new component models, or latest versions thereof, a redesigned coupling interface, 123 complemented by a new CMake build infrastructure, runtime environment and model setup scripts. Furthermore, TSMP2 124 retains the possibility to run component models standalone or in various coupling configurations. Component models may 125 be upgraded to their latest versions to stay up-to-date with new features. With TSMP2, the COSMO atmospheric model has 126 been replaced by one of the latest ICON versions (Pham et al., 2021; Zängl et al., 2015), the Community Land Model v3.5 127 by the encore Community Land Model, a fork of the land surface model CLM5 (Lawrence et al., 2019) for standalone and 128 coupled CLM use. Terrestrial hydrology is still simulated with the integrated hydrologic model ParFlow (Ashby and 129 Falgout, 1996; Kollet and Maxwell, 2006; Kuffour et al., 2020) in one of the latest versions. Technically, model coupling is 130 via the external OASIS3-MCT coupler (Craig et al., 2017), albeit using a revised coupling approach.

131

132 Here we introduce the new TSMP2 RESM with the aim to give a detailed description of the model system, explain the 133 coupling approaches implemented, show-case its basic functionality, and briefly present a typical intended application 134 example. Beyond the coupled model system itself, TSMP2 provides a comprehensive platform that includes a 135 build-infrastructure, supporting software tools for model setup, run-control, and post-processing, along with complete 136 example experiments. This makes TSMP2 readily accessible on GitHub for community use and further development.

137

138 This model descriptor study is organized as follows: Section 2 introduces the TSMP2 component models. Section 3 explains 139 the coupling interface and the component model communication. Section 4 provides evidence of the functioning of the 140 coupling with an idealized test case, including performance considerations. In Section 5, TSMP2 is applied with a real data 141 case for regional climate scenario simulations in line with the CORDEX-CMIP6 dynamical downscaling experiment 142 protocol. Section 6 deals with TSMP2 computational efficiency, while Section 7 provides a short overview on the TSMP2 143 platform functionalities and tools. Last, Section 8 concludes this model overview with open aspects and an outlook to 144 upcoming developments.

## 145 2. TSMP2 model structure and component models

146 The TSMP model system consists of an atmospheric model, a land surface model and an integrated hydrological model
147 coupled via an external coupler.





# 148 2.1 Atmospheric model – ICON

The Icosahedral Nonhydrostatic (ICON, Zängl et al., 2015) model is a unified state of the art numerical weather prediction and climate modeling system that solves the fully compressible non-hydrostatic Navier-Stokes equations on the sphere. A set of physical parameterisations is included, which accounts for the effect of motions that fall below a chosen horizontal mesh size. Depending on its application, ICON is able to run on two different physical packages: Atmosphere Earth System (AES) physics and Numerical Weather Prediction (NWP) physics. ICON-NWP is used for global and regional weather forecasting by the German weather service (DWD) and regional climate modelling (Pham et al., 2021). For small-scale application there is also a large eddy model (ICON-LEM, Dipankar et al., 2015), which uses a planetary boundary layer (PBL) scheme based on Smagorinsky (1963) available for the NWP physics package.

157

158 In contrast to the predecessor COSMO (Baldauf et al., 2011), the ICON is a multi-scale modelling framework designed to 159 run in global, regional (limited-area), convection-permitting and large-eddy simulation configurations, all with consistent 160 dynamical cores. ICON utilizes a icosahedral (triangular) grid system that guarantees consistent resolution worldwide, 161 thereby circumventing the pole singularities typically associated with latitude-longitude grids. The parameterisations of the 162 NWP physics package were selected from various sources, in particular from the COSMO model and the IFS model. 163 Compared to its predecessor, the physical parameterisations have been enhanced, resulting in better prediction quality 164 (Pham et al., 2021; Zängl et al., 2015).

165

166 ICON is jointly developed by the ICON partnership consisting of the German Meteorological Service (DWD), the Max 167 Planck Institute for Meteorology (MPI-M), German Climate Computing Center (DKRZ), Karlsruhe Institute of Technology 168 (KIT) and the Center for Climate Systems Modeling (C2SM). The ICON model can run on CPU and GPU infrastructure 169 (Herten et al., 2024). The ICON component is open source and under the 3-clause BSD license. More information and 170 source code can be found at https://icon-model.org and https://github.com/HPSCTerrSys/icon-model\_coup-oas.

# 171 2.2 Land surface model – eCLM

172 The newly integrated land surface model eCLM is based on the Community Land Model (CLM; Lawrence et al., 2019) that 173 has been developed to simulate land surface processes and interactions with the atmosphere by the National Center for 174 Atmospheric Research (NCAR). CLM v5.0 incorporates intricate representations of land surface processes, such as 175 photosynthesis, various biogeochemical cycles, energy exchange, and hydrology. The model allows for the examination of 176 different land management practices and their impacts on ecosystems, making it a valuable tool for studying climate change, 177 land use change, and natural resource management.

178

179 eCLM is a fork of Community Land Model v5.0 for standalone usage removing the dependencies to the Community Earth 180 System Model (CESM) and developed with minimal dependencies maintained within the Research Centre Jülich. CLM 181 code functionalities remain unmodified besides additional features implemented in the TSMP context. More information 182 and source code is available at https://github.com/HPSCTerrSys/eCLM.

183

**184** Compared to its predecessor CLM3.5 used in TSMP1, eCLM introduces dynamic land unit transitions, a more detailed **185** hydrology and snow system, and mechanistic plant hydraulics incorporating hydraulic redistribution. The biogeochemistry





186 module features modernised nitrogen (N) cycling and leaf physiology with flexible stoichiometry and N optimisation, while 187 a prognostic crop model adds realistic irrigation and fertilisation dynamics. Compared to the native LSMs of the ICON 188 model used as default LSM model of ICON, JSBach and TERRA-ML, the eCLM model includes a more sophisticated soil 189 hydrology representation, an interactive crop model incorporating fertilisation and irrigation, and the ability to depict 190 transient land cover change and dynamic vegetation.

## 191 2.3 Subsurface hydrological model - ParFlow

192 ParFlow is a parallel, integrated hydrology model (IHM), see (Kuffour et al., 2020) for extensive introduction and overview.

193 With the means of Parflow, dynamic two-way groundwater surface water interactions and intermittency in streamflow can

194 be simulated in a continuum approach. ParFlow solves 2D dynamic surface and 3D subsurface flow by the usage of

195 simplified shallow water equations, implicitly coupled to Richards' equation. The Richards equation is discretized in space

196 and time, respectively, using a cell-centered finite-difference scheme and an implicit Eulerian scheme. It is able to simulate

197 a stretched vertical resolution, allowing for shallow vertical layers close to the surface and deep confined and unconfined

198 aquifers.

199

200 The model is exascale-ready and can be run on CPUs and GPUs (Burstedde et al., 2018; Herten et al., 2024; Hokkanen et 201 al., 2021). The ParFlow model is an open-source code under LGPL license available at https://github.com/parflow/parflow, 202 where more information can be found.

#### 203 2.4 Coupler infrastructure – OASIS3-MCT

204 The OASIS coupler (Craig et al., 2017; Valcke, 2013) allows the synchronized exchange of coupling information between 205 the component models and is developed by the Centre Européen de Recherche et de Formation Avancée en Calcul 206 Scientifique (CERFACS) and the Centre National de la Recherche Scientifique - Institut Pierre Simon Laplace 207 (CNRS-IPSL). The fully parallel implementation of coupling field regridding and exchange is provided by OASIS3-MCT, 208 which is the OASIS coupler interfaced with the Model Coupling Toolkit (MCT, Larson et al., 2005) from the Argonne 209 National Laboratory. OASIS3-MCT is widely used for Earth system modelling e.g. in EC-Earth model, CNRM-CM or 210 GCOAST-AHOI (Döscher et al., 2022; Ho-Hagemann et al., 2024; Voldoire et al., 2019). The software is open source and 211 licensed under the GNU Lesser General Public License (LGPL). Its source code is available at 212 https://gitlab.com/cerfacs/oasis3-mct

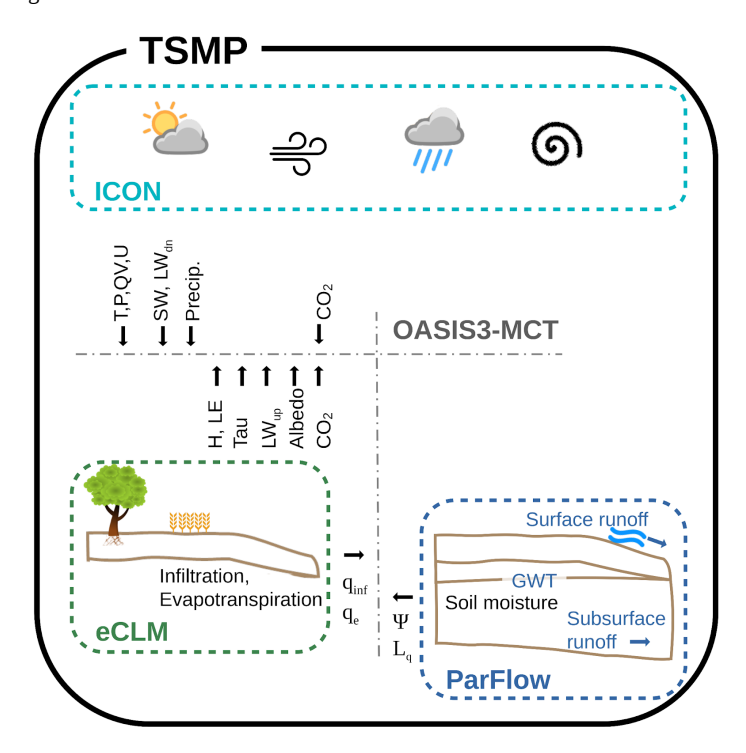
## 213 3. Coupling between component models

214 TSMP2 adopts a multiple program multiple data (MPMD) architecture (Gropp et al., 1999), in which different executables 215 run concurrently on separate processors and exchange information via in-memory MPI-communication during runtime. This 216 design is most suitable for independently developed code such as the TSMP component models involved, and it follows the 217 design of the previous TSMP version. There is a high modularization of TSMP between the component models for different 218 component configurations, allowing for interaction between just two components (ICON-eCLM, eCLM-ParFlow) or all 219 three components (ICON-eCLM-ParFlow), and ICON, eCLM, or ParFlow can even be compiled and run as stand-alone 220 independent models within the TSMP framework (Figure 1). In a coupled mode states and fluxes are passed between the





- 221 component models, i.e., the coupled component models in this case replace the default inputs along the coupling interfaces.
- 222 For example, upper boundary conditions in eCLM may be prescribed without feedback in standalone mode, or provided by
- 223 ICON in a coupled configuration.



224

225 Figure 1: Schematic of the TSMP2 coupled model system. The component models for the atmosphere (ICON), the land surface 226 (eCLM), and the subsurface (ParFlow) are coupled via the external coupler and driver OASIS3-MCT. The following quantities 227 are sent from ICON to eCLM: Temperature at lowermost model level (T), pressure at lowermost model level (P), specific 228 humidity at lowermost model level (QV), horizontal wind speed at lowermost model level (V,U), incident shortwave radiation at 229 surface (SW), longwave downward radiation at the surface (LW), precipitation rate (Precipitation, rain and snow), carbon 230 dioxide (CO2, optional). From eCLM to ICON: Sensible heat flux (H), latent heat flux (LE), momentum flux (Tau), longwave 231 upward radiation at surface (LW), albedo and carbon dioxide (CO2, optional). From eCLM to ParFlow: Infiltration flux ( $q_{inf}$ ). 232 From ParFlow to eCLM: Liquid water content ( $L_0$ ) and the pressure head ( $\Phi$ ).

233

234 TSMP2 is open-source under MIT license and the code is available at https://github.com/HPSCTerrSys/TSMP2. The model 235 system itself as well as its components are open-source. ParFlow and ICON have GPU capabilities, so that heterogeneous 236 applications or even the usage of modular supercomputing infrastructure (MSA) is possible.

## 237 3.1 Flux coupling

238 The primary purpose of OASIS3-MCT (Craig et al., 2017) is the ability to interpolate and exchange the coupling fields 239 between components in memory to form a coupled system. OASIS3-MCT is a coupling library that is compiled and linked 240 to the component models. OASIS3-MCT governs the overall execution and is managed by its own namelist called 241 namcouple. The underlying communication is done via the Model Coupling Toolkit (MCT; Larson et al., 2005). MCT





242 handles the parallel communication and mapping details, thus communication between processors is only activated when

243 needed via a communication scheduler and allows for rank to rank communication. Thus, OASIS3-MCT leads to an

244 efficient exchange of fields with big model domains. Only the overlapping patches exchange information in memory;

245 MPI\_Allgather operations are not required. Each component model has its own MPI communicator and a distinct set of

246 processors. We are using the version 5.0 of OASIS3-MCT available at https://gitlab.com/cerfacs/oasis3-mct.

## 247 3.2 Atmosphere – land surface interface

248 The atmospheric model ICON contains a default land surface model, TERRA-ML (Schrodin and Heise, 2001; Schulz and

249 Vogel, 2020) to provide the lower boundary condition for the atmosphere. TERRA-ML has a rather simplistic representation

250 of the land surface (Pitman, 2003). Depending on user needs, a more process-based representation of vegetation is needed

251 including human land management, ecological models and biogeophysical and biogeochemical processes. In TSMP2, the

252 eCLM LSM replaces the built-in default subroutine-coupled LSM of ICON.

253

254 The atmospheric state of the atmospheric model ICON at its lowest level and current time step is used as the forcing term

255 for eCLM. eCLM then computes the surface energy fluxes, momentum fluxes, albedo, outgoing longwave radiation, and

256 carbon dioxide, which are used as lower boundary conditions in ICON. The coupling between the component models is

257 explicit in time. Sending and receiving of exchanged quantities is done in the component model time loop. The processing

258 of coupled quantities is done in the physics modules of ICON and eCLM (see figure 2 a).

259

260 With TSMP three atmosphere-landsurface coupling approaches are implemented and tested extensively; the default is the

261 fixed flux coupling approach. Flux calculation with ICON-eCLM is determined by the following equations:

262

**263** 
$$H_0 = -\rho c_p |v_h| C_\theta (\theta_{ke} - \theta_s)$$

264 
$$LE_0 = -\rho L_v |v_h| C_q (q_{v,ke} - q_{v,s})$$

$$M_{i,0} = -\rho \, C_M \, |v_h| \, u_{i,ke}$$

267 where  $H_0$  and  $LE_0$  are the sensible and latent heat flux.  $M_0$  is the momentum flux.  $\rho$  is the air density.  $L_v$  is the latent

268 heat for evaporation,  $^{C_p}$  is the specific gas constant for constant pressure,  $^{v_h}$  is the horizontal wind speed,  $^{C_{\theta}}$ ,  $^{C_q}$ , and

269  $C_M$  are the exchange coefficients for heat, moisture and momentum,  $q_{v,ke}$  is the specific humidity at the lowermost

270 atmospheric level and  $u_{i,ke}$  is the wind speed at the lowermost atmospheric level, while  $q_{v,s}$  and  $\theta_{v,s}$  are specific humidity

**271** and temperature at the surface.

272

273 In the original coupling approach proposed, TSMP1 uses the flux inversion approach; where the surface energy and

274 momentum fluxes are coupled ( $H_0$ ,  $LE_0$ ,  $M_0$  in Eq. 1), and based on these fluxes the surface exchange coefficients are

275 used ( $C_{\theta}$ ,  $C_{q}$ ,  $C_{M}$  in Eq. 1), which are in turn used to update the atmospheric states of the lowermost layer (Shrestha et

276 al., 2014). This flux coupling was also originally used with TSMP1. But this coupling approach, namely flux inversion





277 approach, shows weaknesses during transition phases around sunrise and sunset with large changes in energy flux densities,

278 because of unbounded exchange coefficients.

279 Hence, a new coupling scheme was implemented in TSMP1 to ensure numerical stability, where the exchange coefficients

280 are directly coupled instead of the surface energy and momentum fluxes. The direct coupling of exchange coefficients has

281 the advantage of being stable by design but has some drawbacks in the energy and mass conservation between the

282 components.

283 Therefore, a third approach was implemented and is now the default in TSMP2. With the fixed flux coupling approach, the

284 surface energy and momentum fluxes between the atmosphere and land surface are coupled directly and kept constant

285 between the coupling time steps. The fixed flux coupling approach is energy and mass conservative by design, but not

286 necessarily numerically stable. However, coupling time steps below 1 hour generally shows numerical stability (see section

287 4.3).

288

289 ICON can be applied in Large Eddy Model (LEM) for high-resolution simulations and a numerical weather prediction

290 (NWP) mode for climate simulations. Both modes of ICON can be used coupled with eCLM within TSMP2. However, the

291 update of the ICON atmospheric states depends on the used mode and connected Planetary Boundary Layer (PBL) and

292 transfer schemes.

293

294 In LEM mode, the Smagorinsky PBL scheme is a LES scheme (Dipankar et al., 2015). The Smagorinsky PBL scheme uses

295 Dirichlet boundary conditions at the top and bottom boundaries. Thus, the update of the temperature, humidity, and wind

296 speed state of the lowermost half level of ICON is done by directly using the surface energy and momentum fluxes. The

297 transfer scheme based on Louis (1979) is switched off.

298

299 In the NWP mode, the turbdiff PBL scheme is a Turbulent Kinetic Energy (TKE) based scheme based on the level 2.5 of

300 Mellor and Yamada (1982) (Raschendorfer, 2001). The Turbdiff PBL scheme uses in its core von-Neumann boundary

301 conditions for the bottom boundary conditions. The update of temperature, humidity and wind is done based on the

302 lowermost full level of ICON. The surface energy and momentum fluxes need to be transferred to the lowermost half level

303 state variables. The transfer scheme (turbtran) is TKE based, similar to the turbdiff.

304

305 In addition to the surface energy and momentum fluxes, the land surface temperature, specific humidity of the land surface,

306 direct and diffuse albedo as well as outgoing longwave radiation are transferred from eCLM to ICON. In turn, eCLM

307 receives from ICON the lowermost air temperature, wind speed, specific humidity, rain and snow precipitation rate, surface

308 pressure and incoming shortwave and longwave radiation, and measurement height.

309

310 The exchanged variables are passed between the component models at grid cell level. The subgrid hierarchy at patch level

311 in the land surface component is aggregated to grid scale before coupling with the atmosphere or the integrated hydrological

312 model. It is assumed in the coupling of the compartments that every compartment acts on the same topography. The lateral

313 boundary points In the limited area mode of ICON are excluded from the coupling with the land surface model.

314





315 Compared to TSMP1, additional updates include the exchanged quantities to improve the energy and mass conservation 316 between the two compartments. Snow and rain precipitation are coupled separately in TSMP2, so that eCLM can treat each 317 type of precipitation separately.

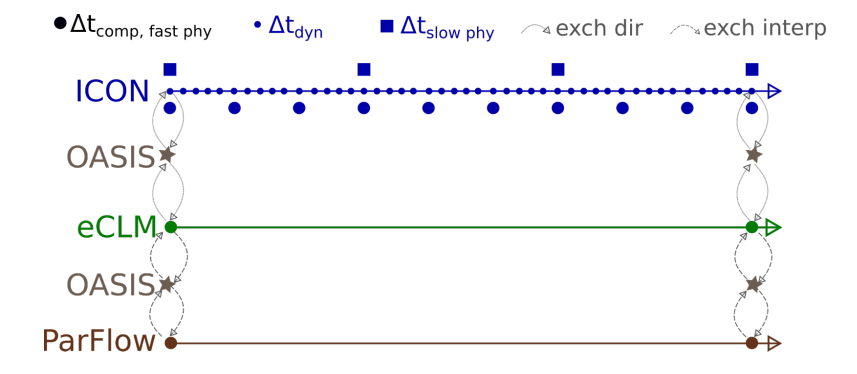
#### 318 3.3 Land surface – subsurface interface

319 Most of the land surface models, including eCLM only act in the vertical dimension. By taking into account the lateral flow 320 of the surface and subsurface hydrological flow, the model can capture the complete terrestrial hydrological cycle. To 321 achieve this coupling, the infiltration flux and root water uptake flux are passed from eCLM to ParFlow, and accounted as 322 sink/source terms of the Richards equation. The pressure potential is passed from ParFlow to eCLM and replaces the 1D 323 Richards solver in eCLM. ParFlow typically has more vertical layers, as it reaches deeper than eCLM. The vertical 324 discretisation for those vertical levels that overlap between eCLM and ParFlow is enforced to be the same for both models, 325 as no vertical interpolation is applied. Note, soil freezing and thawing processes are currently ignored in the interface and 326 will be incorporated in an ensuing development step.

#### 327 3.4 Component model communication

328 TSMP2 employs the OASIS3-MCT coupler to orchestrate the exchange of data fields between components at user-defined 329 coupling intervals, ensuring temporal synchronization and consistent boundary conditions across component models. Each 330 component operates as a separate executable, often on distinct subsets of computing units (e.g., processors), enabling 331 concurrent execution and scalability and each component performs its individual I/O operations. This Multiple Program 332 Multiple Data (MPMD) approach enables efficient resource allocation and concurrent execution, enhancing scalability on 333 distributed-memory systems. Communication between models occurs via parallel, MPI-based field exchanges, configured 334 through coupling metadata that defines variable mappings, interpolation methods, and coupling frequencies via the coupler, 335 which also governs the execution.

336 337 (a)

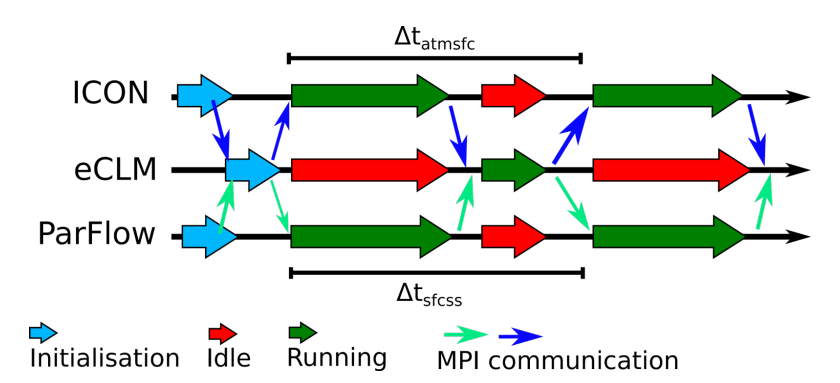


338339





340 (b)



342 Figure 2: (a) Schematic of time sequence of computations and coupling processes in TSMP2, showing one coupling cycle. Lines
343 represent the simulation timeline. (b) Schematic of the synchronization and communication structure. Black lines represent
344 wallclock timelines. While ICON and ParFlow initialize, eCLM is waiting. eCLM receives variables first from ICON and then
345 from ParFlow. While eCLM is running, ICON and ParFlow are idle and vice versa. eCLM sends first to ICON before sending to
346 ParFlow.

347

341

348 When synchronising component models in externally coupled systems, such as TSMP2, governance of the overall execution 349 is required as each component model operates with its own numerical schemes and methods. To ensure that the information 350 is consistent across the component models, there are both asynchronous and sequential coupling elements. Figure 2 shows 351 the coupling frequency synchronization and communication structure within TSMP2. While the initialisation between the 352 atmospheric and hydrological component is independently performed, the land surface component is initialized using the 353 input from the other components. After initialization, the exchanged fields are sent to ICON and ParFlow. Each coupling 354 time step is performed to run ICON and ParFlow asynchronously, while eCLM is run sequentially. After ICON and ParFlow 355 complete their respective time steps while eCLM remains idle, both models send their state variables to eCLM, which then 356 carries out its time step, completing a full coupling time step. The sequential coupling approach ensures the time 357 synchronisation across all component models.

358

359 The coupling time step can interfere with the parameterisation, especially the radiation calculation in ICON. These 360 parameterisations, not performing every time step, are called slow physics and their calling frequency can be set by the 361 ICON namelist. The coupling sequence remains unchanged when performing simulations with two component models. If 362 there is only one, standalone component model, the external coupler is not used.

## 363 4. Proof of coupling concept via idealized test case

364 To explore TSMP2's coupling behavior under simplified, controlled conditions we use an idealized test case. With this test 365 case we can demonstrate TSMP2 functionalities and its usefulness to investigate complex subsurface-surface-atmosphere 366 interactions.

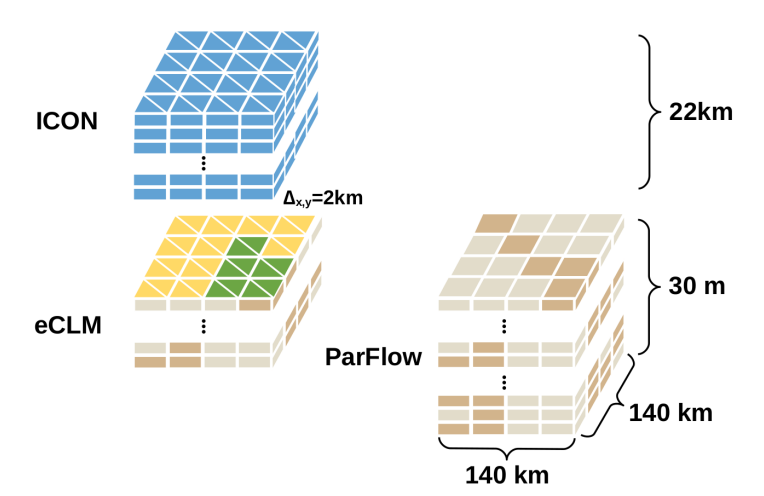




#### 367 4.1 Experimental design

368 The simulation setup uses horizontally homogeneous initial conditions. The simulation time is 24 hours. A periodic 369 boundary condition is used in the X and Y direction for ICON, while a flat terrain is set for ParFlow, so there is no 370 gravity-driven lateral flow. ICON and eCLM operate on the same icosahedral grid while ParFlow operates on a cartesian 371 grid. The horizontal grid spacing is 2 km for all component models and covers an area of 140 x 140 km². In ICON, the 372 vertical grid spacing is staggered from the surface up to a height of 22 km with 50 layers. eCLM's subsurface model grid 373 extends to a depth of 8.5 m with 20 hydrological active layers, and 30 layers for ParFlow to a depth of 30 m, respectively. 374 Figure 3 summarizes the domain setup. The model time step of ICON is 10 seconds, the coupling time step is 600 seconds, 375 which is also the model time step of eCLM and ParFlow.

376



377

378 Figure 3: Setup of TSMP2 component models for the idealised domain. ICON and eCLM run on the same triangular horizontal 379 grid, while ParFlow covers the same area on a rectangular grid, resulting in half of the horizontal grid elements compared to 380 ICON and eCLM.

381

382 The atmosphere is initialized with an idealized vertical profile with a constant lapse rate of 0.6K/100m. Surface, vegetation, 383 and atmospheric temperature at the lowermost model level are initialized at 290 K everywhere. The solar insolation follows 384 the diurnal cycle at 50°N on the 1st of July. We run an ensemble with four members: The volumetric soil moisture is either 385 set to  $\theta$ s=0.11 or  $\theta$ s=0.3 and the land cover is either all grass or forest.

## 386 4.2 Proof of functionality

387 A functionality test between the compartment models within TSMP2 is a critical step to ensure the integrity and reliability
388 of the coupled system. The modular architecture of TSMP2 allows for an independent execution and a flexible coupling
389 configuration of the atmospheric, land surface, and hydrological models; therefore it is essential to verify that data
390 exchange, temporal synchronization, and physical feedback between the component models operate as intended. Such a test
391 confirms that variables are correctly passed, remapped, and conserved across interfaces and to identify potential
392 communication errors, unit mismatches or unintended time lags between the compartments. As we use a fixed flux coupling

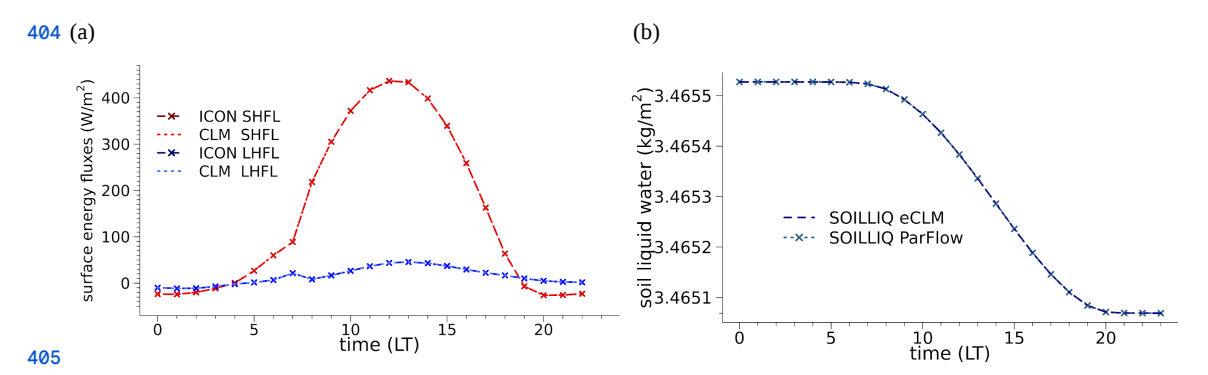




393 approach, any difference between the exchanged fluxes should only originate from the remapping (see Section 3.2 and 3.3).
394 The energy and mass budgets between the coupled compartments is consistent.

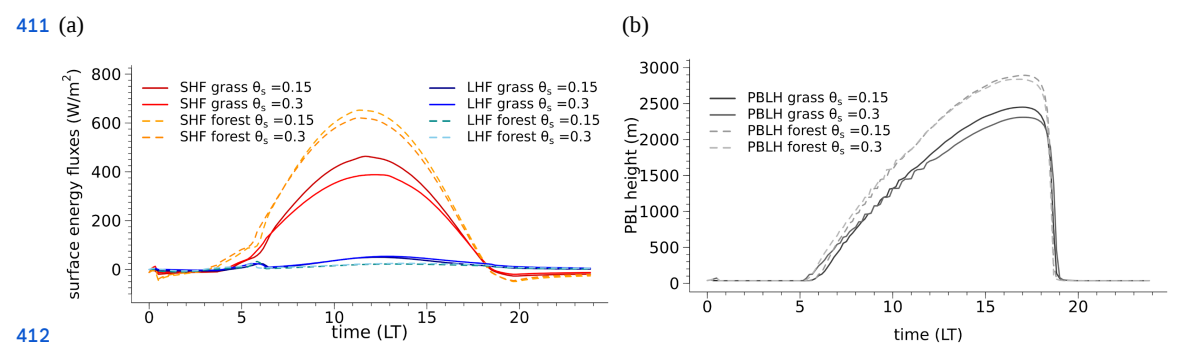
396 Figure 4 shows a comparison of the exchanged fluxes and states of the compartment models using the output from each 397 component model. The surface energy and water balances are central to the interactions between the atmosphere and the 398 land surface. The surface energy fluxes of ICON and eCLM in Figure 4a illustrate that variables pass the coupler interface 399 between ICON and eCLM unmodified, as expected. The flux partitioning reflects the diurnal cycle. The liquid water content 400 (Figure 4b) in the soil layer between 0.02-0.06m of eCLM and ParFlow match as well. Please note that the lines exactly 401 overlap. The decrease is due to the evapotranspiration. Because two grid elements of eCLM exactly match one ParFlow grid 402 element (see Figure 3) this also demonstrates the consistent interpolation between the eCLM and ParFlow grids.

403



406 Figure 4: Comparison of model domain average fluxes (a) and states (b) passed between the TSMP2 compartment models. (a) 407 ICON (long dashes) and CLM (short dashes) sensible (SHFL) and latent (LHFL) heat flux at the surface [W m<sup>-2</sup>]. (b) eCLM (long 408 dashes) and ParFlow (short dashes) liquid water content between 0.02-0.06m depth [kg m<sup>2</sup>]. Please note the lines overlap exactly. 409 Shown is the experiment ensemble member land cover for grass, clay loam soil texture, and an initial soil moisture of  $\theta$ s =0.11.

410



413 Figure 5: As in Figure 4, for land cover grass and Needleleaf temperature evergreen tree (forest) and initial soil moisture of 414  $\theta$ s =0.11 and  $\theta$ s =0.3, and in (b) planetary boundary height identified via the Richardson number.

415

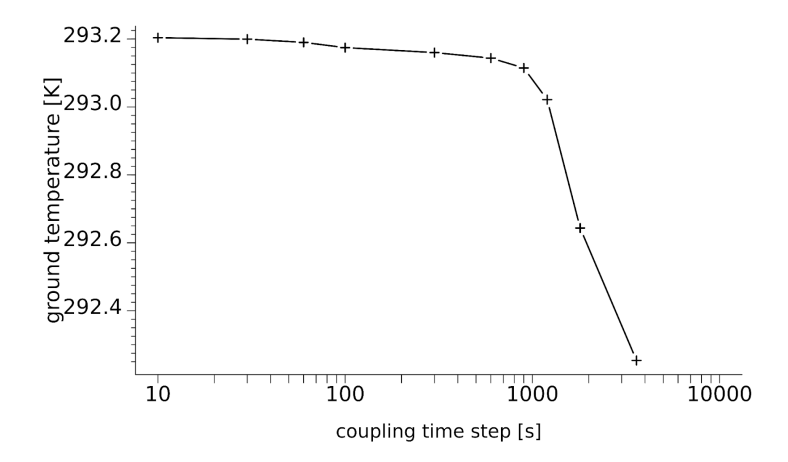
416 Figures 5a and 5b are also from the same ensemble of test simulations, as described above. Here we present the domain 417 averaged surface energy fluxes and planetary boundary layer (PBL) height, respectively, the latter serving as an indicator of





418 the intensity and extent of turbulent mixing and thermodynamic processes occurring within the PBL. Lower soil moisture of 419 ParFlow propagates via eCLM into a smaller sensible heat flux, which results in less buoyancy and thus to a lowering of the 420 PBL height.

#### 421 4.3 Sensitivity to coupling time step



422

423 Figure 6: Ground temperature at the end of the simulation period for different coupling time steps for the idealized test case 424 (Section 4.1) with ICON-eCLM-ParFlow and land cover for grass, clay loam soil texture, and an initial soil moisture of  $\theta$  =0.3.

425 Based on the same idealized test case of section 4.1, additional tests were designed to explore how different coupling 426 interval time steps affect the representation of land-atmosphere interactions in terms of energy fluxes and near-surface air 427 temperature. For all experiments, the model time step for all component models was fixed at 10 seconds, while the coupling 428 time step was modified as indicated in Figure 6. Prior studies (Beljaars et al., 2017; Gross et al., 2018) have shown that 429 large coupling time steps can lead to inaccuracies due to the asynchronous exchange of fast-evolving variables or processes. 430 Our simulations confirm this sensitivity. Longer coupling intervals result in a lowering of temperature compared to shorter 431 coupling time steps (Figure 6).

432 Specifically, the analysis reveals that the optimal coupling time step aligns with the radiation time step, typically on the
433 order of 15 to 30 minutes, depending on model configuration. Coupling intervals longer than one hour lead to a noticeable
434 deterioration in physical consistency, highlighting the importance of tight coupling for realistic representation of non-linear
435 exchange processes. This effect of linearization introduced by operator splitting across component models becomes evident
436 in the model response when the coupling time step is increased and is dependent on the involved processes, which in turn
437 depend on the grid spacing of the model.. These simulations inherently require fine temporal resolution, making sub-hourly
438 coupling both necessary and practical. Therefore, coupling time steps exceeding one hour are not planned for regular use
439 within the platform.





## 440 5. Real test case - CORDEX EUR-12

441 The real case test case shows the ability of the coupled model system to perform as a regional Earth system model. The 442 model domain encompasses the Pan-European continent (Figure 6) and operates at a horizontal resolution of 0.11° 443 (approximately 12.5 km), referred to as the "EUR-12" grid, as part of the COordinated Regional Downscaling EXperiment 444 (CORDEX) project (Gutowski Jr. et al., 2016; Jacob et al., 2020).

#### 445 5.1 Experiment design

446 The ICON model follows the so-called "recommended configuration" of the Climate Limited area Modelling COMmunity 447 (CLMcom) with 50 vertical layers. In this configuration, the eCLM model includes 20 soil layers with a combined depth of 448 8.5 meters. These layers align with the top 20 layers in ParFlow, which extends further with 10 additional layers of 449 increasing thickness toward the base of the model domain, reaching a total depth of 60 meters. ParFlow and eCLM use a 450 time step of 15 minutes, which is also the coupling time step between the compartments, while ICON is running on a 100 451 second time step.

452

453 The external static parameter fields are shared between the component models. The topography data are based on the 454 ASTER dataset. Globcover is used as a land cover data set and mapped to the 17 plant functional type classes of eCLM. 455 ParFlow's hydraulic conductivity parameters are estimated based on soil texture data from the SoilGrids database. Fifteen 456 distinct soil types are used to define permeability, porosity and soil hydraulic conductivity. Figure 7 shows examples of 457 prominent static input data.

458

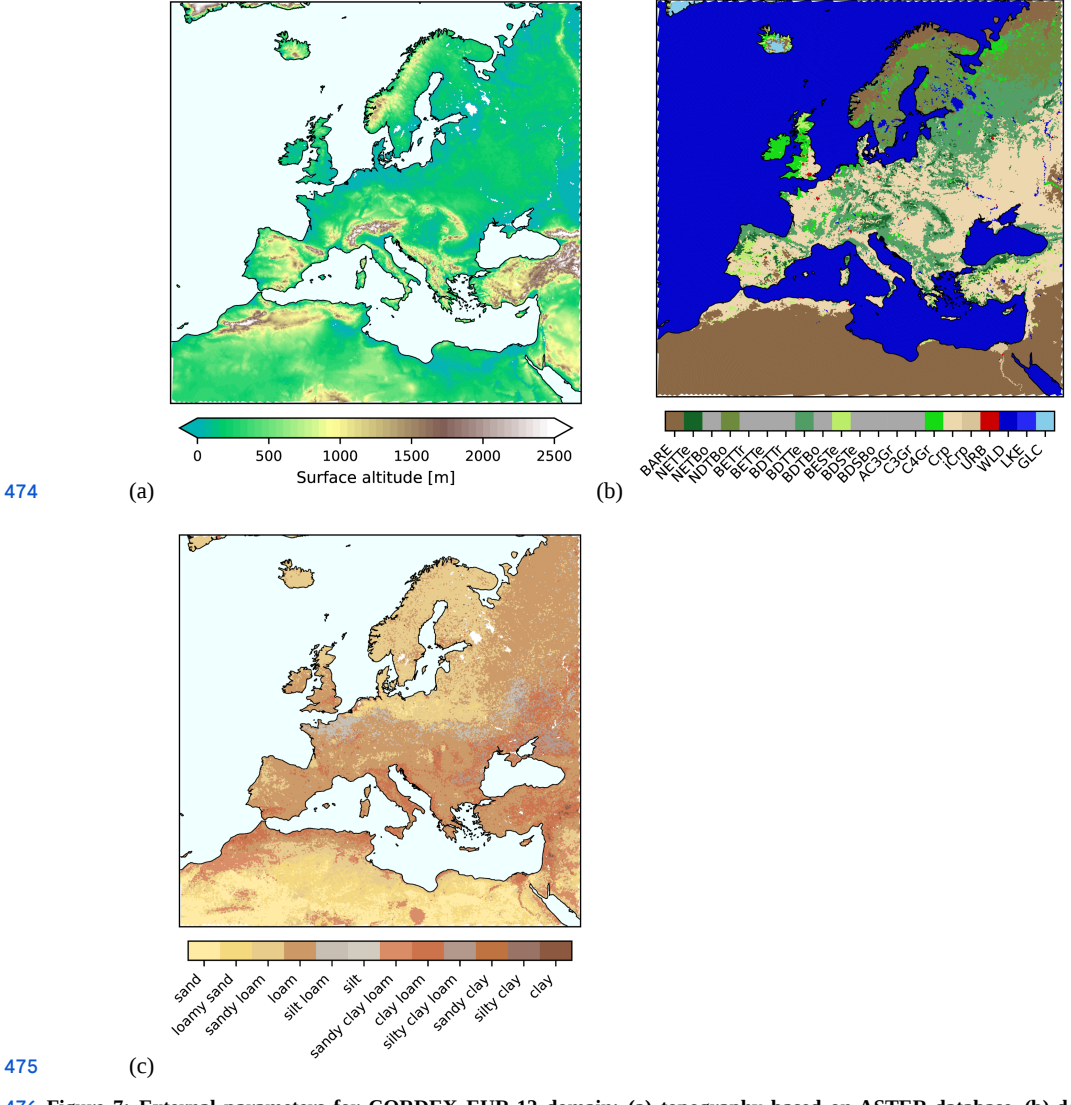
459 The simulation period is July 2017, during which much of Europe experienced a heatwave, and below-average precipitation 460 in some regions. The eCLM is spun-up for 10 years. ParFlow IHM is initialized with a spatially homogeneous water table 461 depth of 2m. The atmospheric boundary conditions for the land surface model spin-up, as well as the initial and lateral 462 boundary conditions, prescribed sea surface temperatures for the atmospheric model, were derived from the ECMWF 463 ERA5 reanalysis (Hersbach et al., 2020).

464

The modular structure of TSMP2 enables a robust validation strategy for its component models by allowing them to be run in standalone, atmosphere-land, land-hydrology, or fully coupled atmosphere-land-hydrology configurations. This flexibility facilitates a targeted evaluation of model system interactions and ensures that there are no coupling-induced artifacts. This stepwise comparison ensures that coupling processes preserve the physical integrity of the individual models and gives confidence in the validity of the fully coupled system. Also, this type of comparison shows the impact of the coupling, i.e., differing results are expected. Since the standalone versions of the component models - such as the ICON atmospheric, eCLM land surface, and ParFlow hydrologic modules - have been in use in a large number of applications and have been independently validated against observational data, their established reliability provides a frame of reference for comparison 473 (e.g., Belleflamme et al., 2023; Lawrence et al., 2019; Pham et al., 2021).







476 Figure 7: External parameters for CORDEX EUR-12 domain: (a) topography based on ASTER database, (b) dominant land 477 cover based on Globecover2009, and (c) soil texture classes in 0.02-0.06m depth based on SoilGrids dataset.

#### 478 5.2 Results

479 This real data case simulation serves as a proof-of-concept, that TSMP2 can be used for such (climate mode) simulations.
480 An analysis of the temporal evolution of 2-m air temperature across all model configurations - standalone, two-model
481 coupling, and fully coupled - reveals a generally consistent behavior in terms of variability and diurnal patterns (Figure 8a).
482 Simulations that incorporate the atmosphere-land surface coupling show systematically lower daily temperatures compared
483 to the other simulations. Furthermore, the fully coupled ICON-eCLM-ParFlow and ICON-eCLM configurations show
484 similar temperature behavior, while the eCLM-ParFlow simulation closely aligns with the standalone eCLM run. This
485 indicates that the inclusion of ParFlow exerts only a modest influence on near-surface temperature relative to the impact of





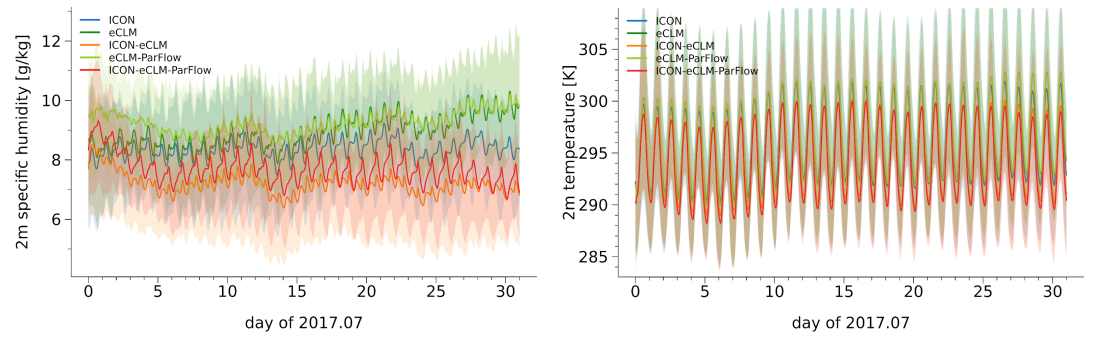
486 the land-surface model. For 2 m specific humidity, higher values are observed at the start of the month due to the inclusion 487 of ParFlow. This effect evens out over the course of the month (Figure 8b).

188

489 The time of the 2m maximum temperature changes with the used LSM. While the 2m maximum temperature with the 490 eCLM LSM is at 14UTC, with ICON and the TERRA-ML LSM it is 1-2 hours earlier, depending on the region (Figure 8b). 491 While the inclusion of ParFlow in the Prudence region of Scandinavia (SC) has no effect, low temperatures are reached in 492 the Iberian Peninsula (IP) and Mediterranean (MD) when the ParFlow IHM component is included. In return, the inclusion 493 of ParFlow results in a more humid atmosphere compared to runs without the IHM component. However, the greatest effect 494 on the 2m specific humidity is observed in an active atmosphere. The daily cycle of 2m specific humidity is driest in the 495 coupled ICON-eCLM simulations, while the simulations with offline atmospheric forcings are wettest (Figure 8b).

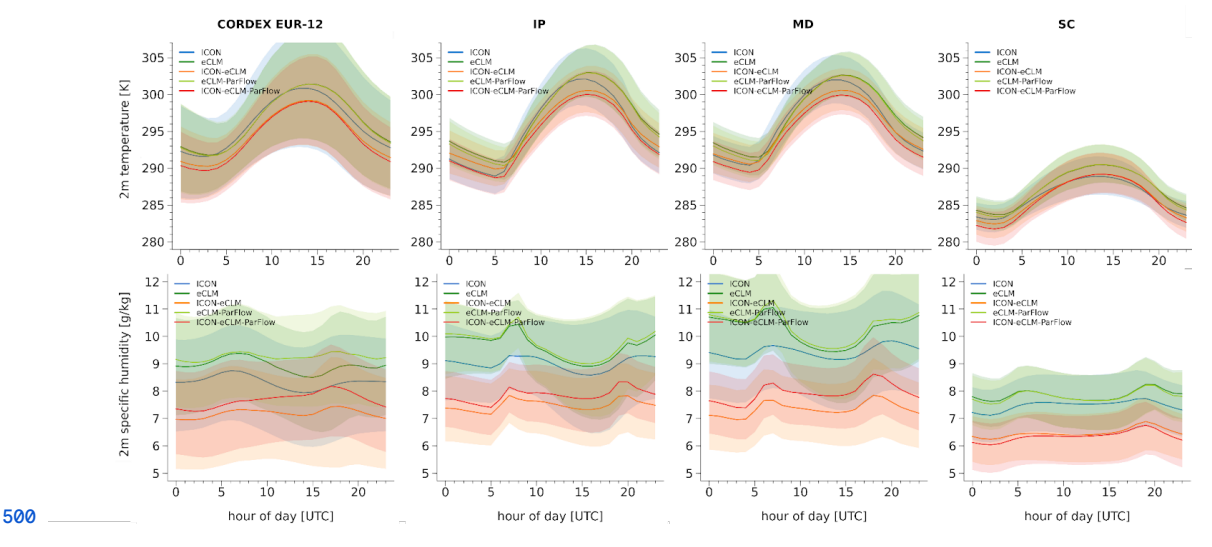
496

497 (a)



499 (b)

498



501 Figure 8: Domain averages (lines) and 25/75% quantiles (shaded area) of the 2m air temperature (a, left column), 2m specific 502 humidity (a, right column) of EURO-CORDEX EUR-12 domain over land for ICON, eCLM, ParFlow, ICON-eCLM, 503 eCLM-ParFlow and ICON-eCLM-ParFlow for July 2017. (b): same as (a) for the diurnal cycle for EURO-CORDEX EUR-12

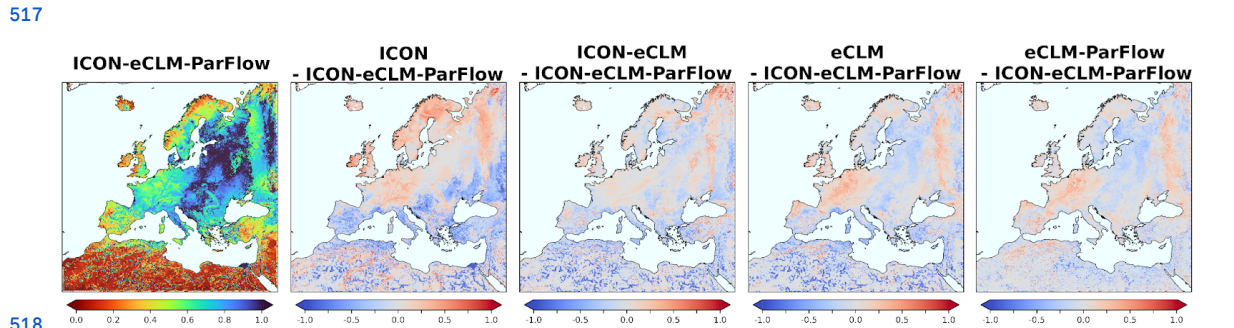




504 domain over land and Prudence regions Iberian Peninsula (IP), Meditarianien (MD) and Scandinavien (SC) after Christensen 505 and Christensen (2007).

506

507 The evaporation fraction (EF) is used as an indicator for characterising atmosphere-land-groundwater coupling (Keune et 508 al., 2016). Figure 9 shows how water and energy fluxes at the surface are clearly affected by the coupling. The 509 ICON-eCLM-ParFlow simulation is used as a reference. As expected, the lowest EF is seen on the African continent, while 510 the highest is seen in Eastern Europe. All simulations show a higher EF over Central Europe compared to the fully coupled 511 reference simulation. Over the Iberian Peninsula, the inclusion of the ParFlow in the coupling leads to a higher EF. 512 ParFlow's impact is still somewhat limited in this simulation, due to the relatively short spinup of the subsurface; 513 ICON-eCLM shows the smallest difference to the reference, also eCLM vs eCLM-ParFlow are very similar. What seems to 514 have the largest impact here on flux partitioning is the inclusion of eCLM that differs strongly from the TERRA in the 515 ICON standalone TSMP2 variant. The LSMs differ for example with respect to their transfer schemes, which is TKE-based 516 in TERRA vs Monin-Obukhov similarity theory-based in eCLM.



519 Figure 9: Evaporative fraction (ratio between latent heat flux and available energy at the land surface) between 06-18 UTC, of 520 EURO-CORDEX EUR-12 domain over land for ICON-eCLM-ParFlow (reference) and ICON, eCLM, ParFlow, ICON-eCLM, 521 eCLM-ParFlow minus reference (from left to right) for 31th July 2017.

# 522 6. Performance and portability

## 523 6.1 Portability

524 A key strength of TSMP2 lies in its high degree of portability across computational environments. The model system is 525 implemented with a modular and standardized infrastructure using a CMake-based build system. CMake enables a 526 standardized and flexible mechanism for configuring, compiling and linking its modular components, ensuring 527 compatibility with a wide range of compilers, libraries and architectures. As a result, TSMP2 can be deployed seamlessly on 528 platforms ranging from local workstations (Linux-based) to high-performance computing (HPC, Tier 0-3) clusters and 529 emerging exascale architectures.

530

531 Different environments are stored in dedicated environment files, each loading the corresponding software environment and 532 compiler settings. These settings can be found in the TSMP2 env directory and can be expanded to any computational



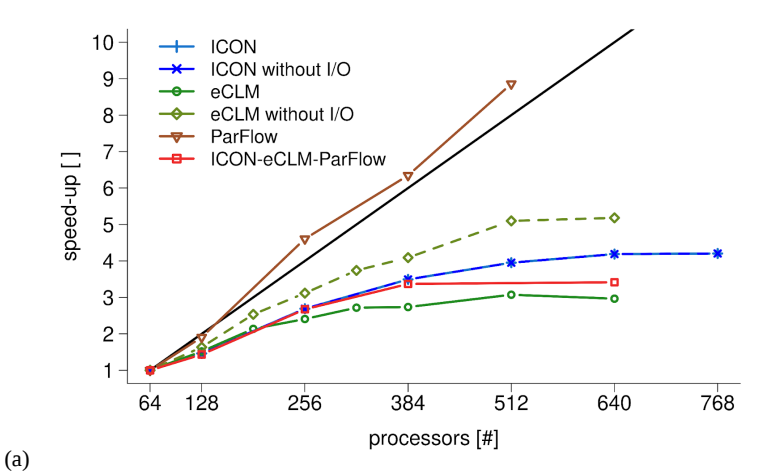


533 environments which are not supported by default. The required dependencies can vary, depending on the installed 534 component model combination.

## 535 6.2 Scalability

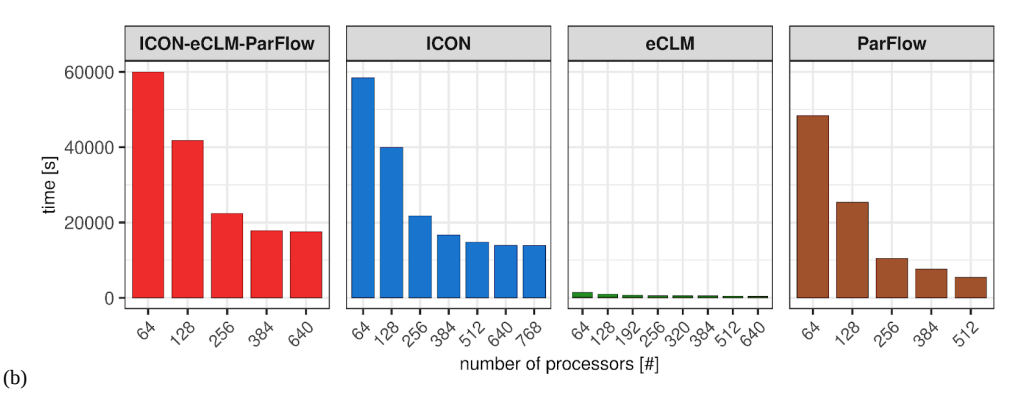
536 The scalability of the system is constrained by the scalability of the component models. A strong scaling study is performed 537 on the JURECA-DC HPC system at the Juelich Supercomputing Centre in Germany, with hybrid MPI-OpenMP 538 parallelization and O2 optimization. JURECA-DC features two AMD EPYC 7742 CPUs per node (128 cores), and 539 InfiniBand HDR100 using an Intel toolchain with a ParaStation MPI implementation (Jülich Supercomputing Centre, 2021). 540 The strong scaling test is based on the EURO-CORDEX EUR-12 climate simulation experiment setup (Section 5.1), 541 including I/O. The target simulation time for such simulations is usually one Simulated Year Per real Day (SYPD). 542 Performance optimisation and scaling studies with a fully coupled system may be complicated (Gasper et al., 2014), and 543 depend on a combination of HPC System, compile time optimisation, model configuration, I/O, model timesteps, coupling 544 time steps, domain or problem size, and grid spacing.

545



546

547



548 Figure 10: Strong scaling for EURO-CORDEX EUR-12 test case for individual component models ICON, eCLM, ParFlow and 549 for the coupled system ICON-eCLM-ParFlow for a simulation time of one month. (a) Speed-up curves of component models and





550 the fully coupled system, black line is ideal speed-up. (b) Bar charts of wallclock times for the fully coupled system (red), ICON 551 only (blue, I/O: turquoise), eCLM only (green, I/O: olive), and ParFlow only (brown).

552

553 Here we apply a simplified scaling experiment where in a first step the optimum scaling of one of the TSMP2 component 554 models, here ICON, is determined; this defines then the wallclock runtime performance envelope for eCLM and ParFlow. In 555 a subsequent step ParFlow is scaled until the ICON runtime stays the same. eCLM scaling follows, according to the same 556 principle. In effect, no component model needs to wait for the others. Thus, for ICON-eCLM-ParFlow, the number of 557 processors specified by ICON remains the same for eCLM and ParFlow at 384 processors.

558

559 ICON shows a moderate strong scaling up to 512 processors. Due to the asynchronous output of ICON (io\_proc\_num=3), 560 the I/O only adds up 10-40 seconds to the total simulation time (20k-60k seconds). Thus, the I/O is not a limiting factor for 561 the scaling of ICON. Whereas, for the eCLM strong scaling, the I/O is a limiting factor, occupying up to 50% of the total 562 runtime for 640 processors. The speed-up of ParFlow follows the optimum line.

563

The simulation time is highest for ICON, which is due to its comprehensive physical parameterisations and fine spatial resolution, which increase the computational effort. ParFlow has less demanding computational requirements (Figure 10b). In contrast, eCLM has significantly faster run times, with simulation times that are orders of magnitude shorter than those of ICON and ParFlow.

568

569 For the coupled system, the number of processors for ParFlow and eCLM is fixed to 384 cores, respectively. The scaling of 570 the coupled system follows the one of the ICON model (Figure 10 a), indicating that this is the limiting component model 571 for the scalability of the system. The simulation time of the coupled model system is larger than the combined simulation 572 times of ICON and eCLM (Figure 2) by 2-5%, which could be attributed to the exchange of fields and load balancing 573 between the three compartments. The reader should keep in mind that in the coupled system, ICON and ParFlow run 574 (partially) concurrently, whereas eCLM runs sequentially before/after ICON and ParFlow. It is therefore expected that the 575 ICON runtime and scalability properties dominate the TSMP2 coupled runtime and scalability.

# 576 6.3 Computational overhead of the coupled model

577 The runtime overhead introduced by the coupled system in TSMP2 amounts to approximately 2–10% compared to the 578 standalone execution of individual component models (Figure 10), if one ignores the increase in computational resources 579 needed. This overhead primarily arises from the coordination and data exchange managed by the coupler, including 580 synchronization at defined coupling intervals. This interpolation step adds computational complexity and communication 581 load beyond the baseline coupling overhead. However, increasing the number of coupled fields, i.e., the volume of 582 exchanged variables, does not have a significant impact on run-time performance, indicating that the communication 583 infrastructure is efficient and not a bottleneck in typical use cases. Overall, TSMP2 maintains strong performance while 584 enabling comprehensive process coupling. In future, a reduction of the runtime overhead could be achieved through the 585 parallel execution of the component models (see Figure 2) and the optimisation of the eCLM output. The I/O of eCLM is 586 the most limiting part in the total runtime of this compartment. Performing output of eCLM after sending the exchanged 587 quantities would be an optimisation for the total runtime of the coupled system. The parallel execution would result in the





588 exchanged quantities having a time shift. However, Marti et al., (2021) showed that using an atmosphere-first approach in 589 parallel execution only resulted in a slight degradation of the simulation results.

## 590 7. TSMP2 framework

591 In order to run simulations, simply providing the coupled model and the build script is not enough. It is also necessary to 592 have static or external parameter fields (topography, land cover, etc.), forcing data, i.e., time-varying boundary conditions, 593 initial conditions, as well as a model configuration, i.e., namelists, and a workflow engine for simulation and data handling, 594 based on a properly installed and maintained runtime environment. In order to handle the authors' own simulation 595 experiments efficiently, aid the development of TSMP2 and support training activities, all of the aforementioned 596 components that make up the TSMP2 framework are provided via public Git repositories. To ensure modularity, which aids 597 in a flexible use and maintenance of the system, each component of the framework has its own Git repository. Together, 598 these components constitute the TSMP2 framework, offering an end-to-end solution that facilitates reproducible workflows, 599 lowers barriers to adoption, and enhances the usability of TSMP for both research and operational applications.

600

601 An overview of the software tools can be found at 602 https://github.com/HPSCTerrSys/.github/blob/main/profile/README.md. The workflow engine provides a summary of the 603 functionalities around simulation experiments by using Git submodule functionality to manage the respective parts to 604 perform a specific simulation ( https://github.com/HPSCTerrSys/TSMP2\_workflow-engine ).

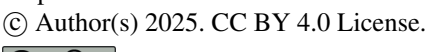
# 605 8. Conclusions and outlook

606 In this model descriptor study, we present the fully modernized free open-source Earth system model, TSMP v2.0.0 607 (TSMP2). In TSMP2 the state of the art atmospheric model ICON (v2024.07), the land surface model eCLM (v0.4) and the 608 integrated hydrologic model ParFlow (v3.14) are coupled via the OASIS3-MCT coupler (v5.0). TSMP2 can be used for a 609 wide range of simulation experiments across a range of spatial and temporal scales. With its focus on a sophisticated 610 terrestrial hydrology representation and explicit treatment of 3D hydrodynamics and groundwater processes and its flexible 611 modular structure, TSMP2 is a valuable tool for studying atmosphere-land-subsurface interactions, water resources 612 questions, and for climate simulations as part of a new class of "increased complexity" model systems, as used in the 613 CORDEX experiment.

614

615 The first version of TSMP (TSMP1) has been in use for over a decade, with a focus on land-atmosphere interaction and 616 water cycle research. TSMP2 enables an even more accurate simulation of the energy and water cycles through the use of 617 new coupling strategies. The state-of-the-art modelling components makes it possible to have a more complete process 618 representation. In this study, the basic coupling functionality of TSMP2 is demonstrated through idealised experiments that 619 also highlight the interconnectivity between groundwater and the atmosphere. A correlation between coupling time step and 620 model parameterisations such as the radiation subroutine calls was found. A real data case simulation over the CORDEX 621 EUR-12 pan European model domain illustrates TSMP2's readiness for regional Earth system modelling.

622





623 As part of the ongoing development TSMP2, a 20-year simulation period is planned for the EUR-12 region at spatial 624 resolutions of 12 km and convection-permitting 3 km. This extended simulation will enable comprehensive evaluation of 625 model performance. The 12 km simulations will provide a robust baseline for regional climate processes forced with ERA5 626 reanalysis data, while the high-resolution 3 km runs will allow for detailed analysis of fine-scale phenomena such as 627 convective precipitation and land-atmosphere feedbacks. Evaluation will be conducted using a suite of observational 628 datasets and reanalyses, ensuring rigorous assessment of atmospheric, land surface, and hydrological components,

629

630 eCLM supports the simulation of bio-geochemical cycles, dynamic vegetation, and a sophisticated representation of urban 631 areas; these features are implemented but not subject to this introduction. In this study, we focused on the hydrological cycle 632 above and below land. To limit complexity and computational demand, we did not include an interactive ocean component, 633 instead prescribed sea-surface temperatures are used. However, achieving a fully integrated Earth system model will require 634 adding an explicit ocean model to TSMP. Oceans contribute to climate regulation through heat storage, carbon 635 sequestration, and biogeochemical cycling, and their coupling with land and atmosphere processes can improve feedback 636 representation, such as carbon exchange and coastal runoff (Heinze et al., 2019).

638 The MPI-based parallelization paradigm also allows for the usage of heterogeneous supercomputers combining CPUs and 639 GPUs, either through Modular Supercomputer Architecture (MSA) execution modes, or the tightly integrated CPU-GPU 640 architecture of superchips such as Grace-Hopper (Caviedes-Voullième et al., 2025). GPUs can be utilized for tasks that 641 require a high level of computation, such as those related to atmospheric and hydrological components. While keeping 642 memory demanding applications, such as the land component, on the CPU.

644 Coupling and synchronisation within terrestrial systems is critical to accurately represent the complex interactions between 645 the atmosphere, land surface and hydrological processes. These components operate on different spatial and temporal 646 scales, necessitating a robust coupling framework that ensures consistent exchange of energy, mass and momentum across 647 compartment interfaces. Previous studies, such as Marti et al. (2021), have shown how coupling synchronisation can 648 influence simulation outcomes and how this influence can be measured using the Schwarz iterative. We plan to adjust the 649 model synchronisation in the future to concurrent coupling by performing an atmosphere- and hydrology-first sequence. 650 This will make a higher frequency between atmosphere and land surface coupling possible.

651

652 This initial presentation of TSMP2 has not yet addressed its capability to operate at the global scale. The ICON atmospheric 653 model is run in many climate and NWP applications globally and eCLM - by original design also the land surface 654 component model of CESM2 (Danabasoglu et al., 2020) - likewise supports global deployment. The hydrologic model 655 ParFlow has recently proven to work globally. Together, these components provide a strong foundation for extending 656 TSMP2 toward fully global Earth system simulations.

657

658 All component models of TSMP2 are under active development, and the modular design of TSMP2 makes such updates 659 easily possible. TSMP2 will continue to be actively developed as a free and open source (regional) Earth system model and 660 in conjunction with a modular framework of auxiliary software tools will be a platform for collaborative research on 661 terrestrial system processes.





#### 662 Code and data availability

- 663 The TSMP2 coupled system can be downloaded from GitHub under this URL: https://github.com/HPSCTerrSys/TSMP2.
- 664 The HPSC-TerrSys competence center GitHub account with all relevant auxiliary tools for TSMP2 is under this URL:
- 665 https://github.com/HPSCTerrSys.
- 666 The complete idealized simulation experiment (initial fields, external parameter fields, model configuration files) from
- 667 Section 4 is available under this URL:
- 668 https://github.com/HPSCTerrSys/simexp\_ideal\_fs-idealnwp\_icon-eclm-parflow\_wfe-case.
- 669 The complete real case simulation experiment from Section 5 is available under this URL:
- 670 https://github.com/HPSCTerrSys/TSMP2 workflow-engine/.
- 671 The ERA5 reanalysis data used as boundary conditions for the real data case in Section 5.2 can be downloaded via the
- 672 Copernicus Climate Change Service, Climate Data Store https://cds.climate.copernicus.eu/datasets.

#### 673 Author contribution

- 674 TSMP2 conceptualization was done by SK with the support of KG and DCV. SP, PR and SB developed the model code,
- 675 HTMHH supported. SP performed the simulations. CH and MvH supported in performing the simulation. AGN and JK
- 676 supported in the framework. KG, DCV and HJHF supported in the design of the experiments. SP prepared the manuscript
- 677 with contributions from all co-authors.

## 678 Competing interests

- 679 The authors declare that they have no conflict of interest. The funders had no role in the design of the study; in the
- 680 collection, analysis, or interpretation of the data; in the writing of the manuscript; or in the decision to publish the results.

## 681 Acknowledgments

- 682 This study is funded by the Deutsche Forschungsgemeinschaft (DFG, German Research Foundation SFB 1502/1-2022 -
- 683 Projektnummer: 450058266). The authors gratefully acknowledge the Gauss Center for Supercomputing e.V.
- 684 (www.gauss-centre.eu) for funding this project by providing computing time through the John von Neumann Institute for
- 685 Computing (NIC) on the GCS supercomputer JUWELS and the supercomputer JURECA-DC (grant no. cjjsc39) at Jülich
- 686 Supercomputing Centre (JSC). S. Brdar gratefully acknowledges the EU funded project DestinE and the project WarmWorld
- 687 Faster funded by the German Federal Ministry of Education and Research.





## 688 Reference

- 689 Arnault, J., Fersch, B., Schrön, M., Bogena, H. R., Franssen, H.-J. H., and Kunstmann, H.: Role of Infiltration on
- 690 Land-Atmosphere Feedbacks in Central Europe: Fully Coupled WRF-Hydro Simulations Evaluated with Cosmic-Ray
- 691 Neutron Soil Moisture Measurements, J. Hydrometeorol., 26, 129–153, https://doi.org/10.1175/JHM-D-24-0049.1, 2025.
- 692 Ashby, S. F. and Falgout, R. D.: A Parallel Multigrid Preconditioned Conjugate Gradient Algorithm for Groundwater Flow
- 693 Simulations, Nucl. Sci. Eng., 124, https://doi.org/10.13182/NSE96-A24230, 1996.
- 694 Avissar, R. and Pielke, R. A.: A Parameterization of Heterogeneous Land Surfaces for Atmospheric Numerical Models and
- 695 Its Impact on Regional Meteorology, Mon. Weather Rev., 117, 2113-2136,
- 696 https://doi.org/10.1175/1520-0493(1989)117%253C2113:APOHLS%253E2.0.CO;2, 1989.
- 697 Baldauf, M., Seifert, A., Förstner, J., Majewski, D., Raschendorfer, M., and Reinhardt, T.: Operational Convective-Scale
- 698 Numerical Weather Prediction with the COSMO Model: Description and Sensitivities, Mon. Weather Rev., 139, 3887–3905,
- 699 https://doi.org/10.1175/MWR-D-10-05013.1, 2011.
- 700 Barlage, M., Chen, F., Rasmussen, R., Zhang, Z., and Miguez-Macho, G.: The Importance of Scale-Dependent Groundwater
- 701 Processes in Land-Atmosphere Interactions Over the Central United States, Geophys. Res. Lett., 48, e2020GL092171,
- 702 https://doi.org/10.1029/2020GL092171, 2021.
- 703 Beljaars, A., Dutra, E., Balsamo, G., and Lemarié, F.: On the numerical stability of surface-atmosphere coupling in weather
- 704 and climate models, Geosci. Model Dev., 10, 977–989, https://doi.org/10.5194/gmd-10-977-2017, 2017.
- 705 Belleflamme, A., Goergen, K., Wagner, N., Kollet, S., Bathiany, S., El Zohbi, J., Rechid, D., Vanderborght, J., and
- 706 Vereecken, H.: Hydrological forecasting at impact scale: the integrated ParFlow hydrological model at 0.6 km for climate
- 707 resilient water resource management over Germany, Front. Water, 5, https://doi.org/10.3389/frwa.2023.1183642, 2023.
- 708 Burstedde, C., Fonseca, J. A., and Kollet, S.: Enhancing speed and scalability of the ParFlow simulation code, Comput.
- 709 Geosci., 22, 347–361, https://doi.org/10.1007/s10596-017-9696-2, 2018.
- 710 Caviedes-Voullième, D., Koh, S.-R., Poll, S., Suarez, E., Arakawa, T., Nakajima, K., and Sumimoto, S.: Portability
- 711 of Multiphysics Applications on Heterogeneous Modular Supercomputers, in: Parallel Processing and Applied
- 712 Mathematics, Cham, 47–62, https://doi.org/10.1007/978-3-031-85703-4\_4, 2025.
- 713 Christensen, J. H. and Christensen, O. B.: A summary of the PRUDENCE model projections of changes in European
- 714 climate by the end of this century, Clim. Change, 81, 7–30, https://doi.org/10.1007/s10584-006-9210-7, 2007.
- 715 Craig, A., Valcke, S., and Coquart, L.: Development and performance of a new version of the OASIS coupler,
- 716 OASIS3-MCT\_3.0, Geosci. Model Dev., 10, 3297–3308, https://doi.org/10.5194/gmd-10-3297-2017, 2017.
- 717 Danabasoglu, G., Lamarque, J.-F., Bacmeister, J., Bailey, D. A., DuVivier, A. K., Edwards, J., Emmons, L. K., Fasullo, J.,
- 718 Garcia, R., Gettelman, A., Hannay, C., Holland, M. M., Large, W. G., Lauritzen, P. H., Lawrence, D. M., Lenaerts, J. T. M.,
- 719 Lindsay, K., Lipscomb, W. H., Mills, M. J., Neale, R., Oleson, K. W., Otto-Bliesner, B., Phillips, A. S., Sacks, W., Tilmes,
- 720 S., Van Kampenhout, L., Vertenstein, M., Bertini, A., Dennis, J., Deser, C., Fischer, C., Fox-Kemper, B., Kay, J. E.,
- 721 Kinnison, D., Kushner, P. J., Larson, V. E., Long, M. C., Mickelson, S., Moore, J. K., Nienhouse, E., Polvani, L., Rasch, P.
- 722 J., and Strand, W. G.: The Community Earth System Model Version 2 (CESM2), J. Adv. Model. Earth Syst., 12,
- **723** e2019MS001916, https://doi.org/10.1029/2019MS001916, 2020.
- 724 Dipankar, A., Stevens, B., Heinze, R., Moseley, C., Zängl, G., Giorgetta, M., and Brdar, S.: Large eddy simulation using the
- 725 general circulation model ICON, J. Adv. Model. Earth Syst., 7, 963–986, https://doi.org/10.1002/2015MS000431, 2015.
- 726 Döscher, R., Acosta, M., Alessandri, A., Anthoni, P., Arsouze, T., Bergman, T., Bernardello, R., Boussetta, S., Caron, L.-P.,
- 727 Carver, G., Castrillo, M., Catalano, F., Cvijanovic, I., Davini, P., Dekker, E., Doblas-Reyes, F. J., Docquier, D., Echevarria,
- 728 P., Fladrich, U., Fuentes-Franco, R., Gröger, M., v. Hardenberg, J., Hieronymus, J., Karami, M. P., Keskinen, J.-P., Koenigk,
- 729 T., Makkonen, R., Massonnet, F., Ménégoz, M., Miller, P. A., Moreno-Chamarro, E., Nieradzik, L., van Noije, T., Nolan, P.,
- 730 O'Donnell, D., Ollinaho, P., van den Oord, G., Ortega, P., Prims, O. T., Ramos, A., Reerink, T., Rousset, C.,
- 731 Ruprich-Robert, Y., Le Sager, P., Schmith, T., Schrödner, R., Serva, F., Sicardi, V., Sloth Madsen, M., Smith, B., Tian, T.,





- 732 Tourigny, E., Uotila, P., Vancoppenolle, M., Wang, S., Wårlind, D., Willén, U., Wyser, K., Yang, S., Yepes-Arbós, X., and
- 733 Zhang, Q.: The EC-Earth3 Earth system model for the Coupled Model Intercomparison Project 6, Geosci. Model Dev., 15,
- 734 2973–3020, https://doi.org/10.5194/gmd-15-2973-2022, 2022.
- 735 Fersch, B., Senatore, A., Adler, B., Arnault, J., Mauder, M., Schneider, K., Völksch, I., and Kunstmann, H.: High-resolution
- 736 fully coupled atmospheric–hydrological modeling: a cross-compartment regional water and energy cycle evaluation,
- 737 Hydrol. Earth Syst. Sci., 24, 2457–2481, https://doi.org/10.5194/hess-24-2457-2020, 2020.
- 738 Furusho-Percot, C., Goergen, K., Hartick, C., Kulkarni, K., Keune, J., and Kollet, S.: Pan-European groundwater to
- 739 atmosphere terrestrial systems climatology from a physically consistent simulation, Sci. Data, 6, 320,
- 740 https://doi.org/10.1038/s41597-019-0328-7, 2019.
- 741 Furusho-Percot, C., Goergen, K., Hartick, C., Poshyvailo-Strube, L., and Kollet, S.: Groundwater Model Impacts
- 742 Multiannual Simulations of Heat Waves, Geophys. Res. Lett., 49, e2021GL096781, https://doi.org/10.1029/2021GL096781,
- **743** 2022.
- 744 Gasper, F., Goergen, K., Shrestha, P., Sulis, M., Rihani, J., Geimer, M., and Kollet, S.: Implementation and scaling of the
- 745 fully coupled Terrestrial Systems Modeling Platform (TerrSysMP v1.0) in a massively parallel supercomputing environment
- 746 a case study on JUQUEEN (IBM Blue Gene/Q), Geosci. Model Dev., 7, 2531–2543,
- 747 https://doi.org/10.5194/gmd-7-2531-2014, 2014.
- 748 Gropp, W., Lusk, E., and Skjellum, A.: Using MPI: Portable Parallel Programming with the Message-Passing Interface, 2nd
- 749 ed., MIT Press, Cambridge, MA, 1999.
- 750 Gross, M., Wan, H., Rasch, P. J., Caldwell, P. M., Williamson, D. L., Klocke, D., Jablonowski, C., Thatcher, D. R., Wood,
- 751 N., Cullen, M., Beare, B., Willett, M., Lemarié, F., Blayo, E., Malardel, S., Termonia, P., Gassmann, A., Lauritzen, P. H.,
- 752 Johansen, H., Zarzycki, C. M., Sakaguchi, K., and Leung, R.: Physics-Dynamics Coupling in Weather, Climate, and Earth
- 753 System Models: Challenges and Recent Progress, Mon. Weather Rev., 146, 3505–3544,
- 754 https://doi.org/10.1175/MWR-D-17-0345.1, 2018.
- 755 Gutowski Jr., W. J., Giorgi, F., Timbal, B., Frigon, A., Jacob, D., Kang, H.-S., Raghavan, K., Lee, B., Lennard, C., Nikulin,
- 756 G., O'Rourke, E., Rixen, M., Solman, S., Stephenson, T., and Tangang, F.: WCRP COordinated Regional Downscaling
- 757 EXperiment (CORDEX): a diagnostic MIP for CMIP6, Geosci. Model Dev., 9, 4087–4095,
- 758 https://doi.org/10.5194/gmd-9-4087-2016, 2016.
- 759 Hartick, C., Furusho-Percot, C., Goergen, K., and Kollet, S.: An Interannual Probabilistic Assessment of Subsurface Water
- 760 Storage Over Europe Using a Fully Coupled Terrestrial Model, Water Resour. Res., 57, e2020WR027828,
- 761 https://doi.org/10.1029/2020WR027828, 2021.
- 762 Hartick, C., Furusho-Percot, C., Clark, M. P., and Kollet, S.: An Interannual Drought Feedback Loop Affects the Surface
- 763 Energy Balance and Cloud Properties, Geophys. Res. Lett., 49, e2022GL100924, https://doi.org/10.1029/2022GL100924,
- **764** 2022.
- 765 Heinze, C., Eyring, V., Friedlingstein, P., Jones, C., Balkanski, Y., Collins, W., Fichefet, T., Gao, S., Hall, A., Ivanova, D.,
- 766 Knorr, W., Knutti, R., Löw, A., Ponater, M., Schultz, M. G., Schulz, M., Siebesma, P., Teixeira, J., Tselioudis, G., and
- 767 Vancoppenolle, M.: ESD Reviews: Climate feedbacks in the Earth system and prospects for their evaluation, Earth Syst.
- 768 Dyn., 10, 379–452, https://doi.org/10.5194/esd-10-379-2019, 2019.
- 769 Hersbach, H., Bell, B., Berrisford, P., Hirahara, S., Horányi, A., Muñoz-Sabater, J., Nicolas, J., Peubey, C., Radu, R.,
- 770 Schepers, D., Simmons, A., Soci, C., Abdalla, S., Abellan, X., Balsamo, G., Bechtold, P., Biavati, G., Bidlot, J., Bonavita,
- 771 M., De Chiara, G., Dahlgren, P., Dee, D., Diamantakis, M., Dragani, R., Flemming, J., Forbes, R., Fuentes, M., Geer, A.,
- 772 Haimberger, L., Healy, S., Hogan, R. J., Hólm, E., Janisková, M., Keeley, S., Laloyaux, P., Lopez, P., Lupu, C., Radnoti, G.,
- 773 de Rosnay, P., Rozum, I., Vamborg, F., Villaume, S., and Thépaut, J.-N.: The ERA5 global reanalysis, Q. J. R. Meteorol.
- 774 Soc., 146, 1999–2049, https://doi.org/10.1002/qj.3803, 2020.
- 775 Herten, A., Achilles, S., Alvarez, D., Badwaik, J., Behle, E., Bode, M., Breuer, T., Caviedes-Voullième, D., Cherti, M.,
- 776 Dabah, A., El Sayed, S., Frings, W., Gonzalez-Nicolas, A., Gregory, E. B., Mood, K. H., Hater, T., Jitsev, J., John, C. M.,
- 777 Meinke, J. H., Meyer, C. I., Mezentsev, P., Mirus, J.-O., Nassyr, S., Penke, C., Römmer, M., Sinha, U., von St. Vieth, B.,





- 778 Stein, O., Suarez, E., Willsch, D., and Zhukov, I.: Application-Driven Exascale: The JUPITER Benchmark Suite, in:
- 779 Proceedings of the International Conference for High Performance Computing, Networking, Storage, and Analysis, Atlanta,
- 780 GA, USA, 1-45, https://doi.org/10.1109/SC41406.2024.00038, 2024.
- 781 Ho-Hagemann, H. T. M., Maurer, V., Poll, S., and Fast, I.: Coupling the regional climate model ICON-CLM v2.6.6 to the
- 782 Earth system model GCOAST-AHOI v2.0 using OASIS3-MCT v4.0, Geosci. Model Dev., 17, 7815-7834,
- 783 https://doi.org/10.5194/gmd-17-7815-2024, 2024.
- 784 Hokkanen, J., Kollet, S., Kraus, J., Herten, A., Hrywniak, M., and Pleiter, D.: Leveraging HPC accelerator architectures
- 785 with modern techniques hydrologic modeling on GPUs with ParFlow, Comput. Geosci., 25, 1579–1590,
- 786 https://doi.org/10.1007/s10596-021-10051-4, 2021.
- 787 Huntington, T. G.: Evidence for intensification of the global water cycle: Review and synthesis, J. Hydrol., 319, 83–95,
- 788 https://doi.org/10.1016/j.jhydrol.2005.07.003, 2006.
- 789 Jacob, D., Teichmann, C., Sobolowski, S., Katragkou, E., Anders, I., Belda, M., Benestad, R., Boberg, F., Buonomo, E.,
- 790 Cardoso, R. M., Casanueva, A., Christensen, O. B., Christensen, J. H., Coppola, E., De Cruz, L., Davin, E. L., Dobler, A.,
- 791 Domínguez, M., Fealy, R., Fernandez, J., Gaertner, M. A., García-Díez, M., Giorgi, F., Gobiet, A., Goergen, K.,
- 792 Gómez-Navarro, J. J., Alemán, J. J. G., Gutiérrez, C., Gutiérrez, J. M., Güttler, I., Haensler, A., Halenka, T., Jerez, S.,
- 793 Jiménez-Guerrero, P., Jones, R. G., Keuler, K., Kjellström, E., Knist, S., Kotlarski, S., Maraun, D., van Meijgaard, E.,
- 794 Mercogliano, P., Montávez, J. P., Navarra, A., Nikulin, G., de Noblet-Ducoudré, N., Panitz, H.-J., Pfeifer, S., Piazza, M.,
- 795 Pichelli, E., Pietikäinen, J.-P., Prein, A. F., Preuschmann, S., Rechid, D., Rockel, B., Romera, R., Sánchez, E., Sieck, K.,
- 796 Soares, P. M. M., Somot, S., Srnec, L., Sørland, S. L., Termonia, P., Truhetz, H., Vautard, R., Warrach-Sagi, K., and
- 797 Wulfmeyer, V.: Regional climate downscaling over Europe: perspectives from the EURO-CORDEX community, Reg.
- 798 Environ. Change, 20, 51, https://doi.org/10.1007/s10113-020-01606-9, 2020.
- 799 Jöckel, P., Kerkweg, A., Pozzer, A., Sander, R., Tost, H., Riede, H., Baumgaertner, A., Gromov, S., and Kern, B.:
- 800 Development cycle 2 of the Modular Earth Submodel System (MESSy2), Geosci. Model Dev., 3, 717–752,
- 801 https://doi.org/10.5194/gmd-3-717-2010, 2010.
- 802 Jülich Supercomputing Centre: JURECA: Data Centric and Booster Modules implementing the Modular Supercomputing
- 803 Architecture at Jülich Supercomputing Centre, J. Large-Scale Res. Facil. JLSRF, 7, A182,
- 804 https://doi.org/10.17815/jlsrf-7-182, 2021.
- 805 Katragkou, E., Sobolowski, S. P., Teichmann, C., Solmon, F., Pavlidis, V., Rechid, D., Hoffmann, P., Fernandez, J., Nikulin,
- 806 G., and Jacob, D.: Delivering an Improved Framework for the New Generation of CMIP6-Driven EURO-CORDEX
- 807 Regional Climate Simulations, Bull. Am. Meteorol. Soc., 105, E962-E974, https://doi.org/10.1175/BAMS-D-23-0131.1,
- 808 2024.
- 809 Keune, J., Gasper, F., Goergen, K., Hense, A., Shrestha, P., Sulis, M., and Kollet, S.: Studying the influence of groundwater
- 810 representations on land surface-atmosphere feedbacks during the European heat wave in 2003, J. Geophys. Res.
- **811** Atmospheres, 121, 13,301-13,325, https://doi.org/10.1002/2016JD025426, 2016.
- 812 Keune, J., Sulis, M., Kollet, S., Siebert, S., and Wada, Y.: Human Water Use Impacts on the Strength of the Continental Sink
- 813 for Atmospheric Water, Geophys. Res. Lett., 45, 4068–4076, https://doi.org/10.1029/2018GL077621, 2018.
- 814 Kollet, S., Gasper, F., Brdar, S., Goergen, K., Hendricks-Franssen, H.-J., Keune, J., Kurtz, W., Küll, V., Pappenberger, F.,
- 815 Poll, S., Trömel, S., Shrestha, P., Simmer, C., and Sulis, M.: Introduction of an Experimental Terrestrial
- 816 Forecasting/Monitoring System at Regional to Continental Scales Based on the Terrestrial Systems Modeling Platform
- 817 (v1.1.0), Water, 10, 1697, https://doi.org/10.3390/w10111697, 2018.
- 818 Kollet, S. J. and Maxwell, R. M.: Integrated surface-groundwater flow modeling: A free-surface overland flow boundary
- 819 condition in a parallel groundwater flow model, Adv. Water Resour., 29, 945–958,
- 820 https://doi.org/10.1016/j.advwatres.2005.08.006, 2006.
- 821 Kuffour, B. N. O., Engdahl, N. B., Woodward, C. S., Condon, L. E., Kollet, S., and Maxwell, R. M.: Simulating coupled
- 822 surface–subsurface flows with ParFlow v3.5.0: capabilities, applications, and ongoing development of an open-source,





- 823 massively parallel, integrated hydrologic model, Geosci. Model Dev., 13, 1373–1397,
- 824 https://doi.org/10.5194/gmd-13-1373-2020, 2020.
- 825 Lahmers, T. M., Gupta, H., Castro, C. L., Gochis, D. J., Yates, D., Dugger, A., Goodrich, D., and Hazenberg, P.: Enhancing
- 826 the Structure of the WRF-Hydro Hydrologic Model for Semiarid Environments, J. Hydrometeorol., 20, 691–714,
- 827 https://doi.org/10.1175/JHM-D-18-0064.1, 2019.
- 828 Larson, J., Jacob, R., and Ong, E.: The model coupling toolkit: A new Fortran90 toolkit for building multiphysics parallel
- 829 coupled models, Int. J. High Perform. Comput. Appl., 19, 277–292, https://doi.org/10.1177/1094342005056115, 2005.
- 830 Lawrence, D. M., Fisher, R. A., Koven, C. D., Oleson, K. W., Swenson, S. C., Bonan, G., Collier, N., Ghimire, B., van
- 831 Kampenhout, L., Kennedy, D., Kluzek, E., Lawrence, P. J., Li, F., Li, H., Lombardozzi, D., Riley, W. J., Sacks, W. J., Shi,
- 832 M., Vertenstein, M., Wieder, W. R., Xu, C., Ali, A. A., Badger, A. M., Bisht, G., van den Broeke, M., Brunke, M. A., Burns,
- 833 S. P., Buzan, J., Clark, M., Craig, A., Dahlin, K., Drewniak, B., Fisher, J. B., Flanner, M., Fox, A. M., Gentine, P., Hoffman,
- 834 F., Keppel-Aleks, G., Knox, R., Kumar, S., Lenaerts, J., Leung, L. R., Lipscomb, W. H., Lu, Y., Pandey, A., Pelletier, J. D.,
- 835 Perket, J., Randerson, J. T., Ricciuto, D. M., Sanderson, B. M., Slater, A., Subin, Z. M., Tang, J., Thomas, R. Q., Val Martin,
- 836 M., and Zeng, X.: The Community Land Model Version 5: Description of New Features, Benchmarking, and Impact of
- 837 Forcing Uncertainty, J. Adv. Model. Earth Syst., 11, 4245–4287, https://doi.org/10.1029/2018MS001583, 2019.
- 838 Louis, J.-F.: A parametric model of vertical eddy fluxes in the atmosphere, Bound.-Layer Meteorol., 17, 187–202,
- 839 https://doi.org/10.1007/BF00117978, 1979.
- 840 Marti, O., Nguyen, S., Braconnot, P., Valcke, S., Lemarié, F., and Blayo, E.: A Schwarz iterative method to evaluate
- 841 ocean-atmosphere coupling schemes: implementation and diagnostics in IPSL-CM6-SW-VLR, Geosci. Model Dev., 14,
- 842 2959–2975, https://doi.org/10.5194/gmd-14-2959-2021, 2021.
- 843 Mbabazi, D., Sehgal, V., and Mohanty, B. P.: Global Terrestrial Water-Energy Coupling Across Scales, Ecohydrology, 18,
- 844 e2743, https://doi.org/10.1002/eco.2743, 2025.
- 845 Mellor, G. L. and Yamada, T.: Development of a turbulence closure model for geophysical fluid problems, Rev. Geophys.,
- 846 20, 851–875, https://doi.org/10.1029/RG020i004p00851, 1982.
- 847 Miguez-Macho, G., Fan, Y., Weaver, C. P., Walko, R., and Robock, A.: Incorporating water table dynamics in climate
- 848 modeling: 2. Formulation, validation, and soil moisture simulation, J. Geophys. Res. Atmospheres, 112,
- 849 https://doi.org/10.1029/2006JD008112, 2007.
- 850 Oleson, K., Dai, Y., Bonan, B., Bosilovichm, M., Dickinson, R., Dirmeyer, P., Hoffman, F., Houser, P., Levis, S., Niu, G.-Y.,
- 851 and others: Technical description of the community land model (CLM), 2004.
- 852 Pham, T. V., Steger, C., Rockel, B., Keuler, K., Kirchner, I., Mertens, M., Rieger, D., Zängl, G., and Früh, B.: ICON in
- 853 Climate Limited-area Mode (ICON release version 2.6.1): a new regional climate model, Geosci. Model Dev., 14,
- 854 985-1005, https://doi.org/10.5194/gmd-14-985-2021, 2021.
- 855 Pitman, A. J.: The evolution of, and revolution in, land surface schemes designed for climate models, Int. J. Climatol., 23,
- 856 479–510, https://doi.org/10.1002/joc.893, 2003.
- 857 Poshyvailo-Strube, L., Wagner, N., Goergen, K., Furusho-Percot, C., Hartick, C., and Kollet, S.: Impact of groundwater
- 858 representation on heat events in regional climate simulations over Europe, Earth Syst. Dyn., 15, 167–189,
- 859 https://doi.org/10.5194/esd-15-167-2024, 2024.
- 860 Primo, C., Kelemen, F. D., Feldmann, H., Akhtar, N., and Ahrens, B.: A regional atmosphere-ocean climate system model
- 861 (CCLMv5.0clm7-NEMOv3.3-NEMOv3.6) over Europe including three marginal seas: on its stability and performance,
- 862 Geosci. Model Dev., 12, 5077–5095, https://doi.org/10.5194/gmd-12-5077-2019, 2019.
- 863 Raschendorfer, M.: The new turbulence parameterization of LM, COSMO Newsl., 1, 89–97, 2001.
- 864 Schlemmer, L., Schär, C., Lüthi, D., and Strebel, L.: A Groundwater and Runoff Formulation for Weather and Climate
- 865 Models, J. Adv. Model. Earth Syst., 10, 1809–1832, https://doi.org/10.1029/2017MS001260, 2018.





- 866 Schrodin, R. and Heise, E.: The multi-layer version of the DWD soil model TERRA\_LM, DWD Offenb. Ger., https://doi.
- 867 org/10.5676/DWD\_pub/nwv/cosmo-tr\_2, 2001.
- 868 Schulz, J.-P. and Vogel, G.: Improving the Processes in the Land Surface Scheme TERRA: Bare Soil Evaporation and Skin
- 869 Temperature, Atmosphere, 11, 513, https://doi.org/10.3390/atmos11050513, 2020.
- 870 Sevault, F., Somot, S., Alias, A., Dubois, C., Lebeaupin-Brossier, C., Nabat, P., Adloff, F., Déqué, M., and Decharme, B.: A
- 871 fully coupled Mediterranean regional climate system model: design and evaluation of the ocean component for the
- 872 1980–2012 period, Tellus, 66, https://doi.org/10.3402/tellusa.v66.23967, 2014.
- 873 Shrestha, P., Sulis, M., Masbou, M., Kollet, S., and Simmer, C.: A Scale-Consistent Terrestrial Systems Modeling Platform
- 874 Based on COSMO, CLM, and ParFlow, Mon. Weather Rev., 142, 3466–3483, https://doi.org/10.1175/MWR-D-14-00029.1,
- **875** 2014.
- 876 Smagorinsky, J.: GENERAL CIRCULATION EXPERIMENTS WITH THE PRIMITIVE EQUATIONS: I. THE BASIC
- 877 EXPERIMENT, Mon. Weather Rev., 91, 99-164,
- 878 https://doi.org/10.1175/1520-0493(1963)091%253C0099:GCEWTP%253E2.3.CO;2, 1963.
- 879 Sulis, M., Meyerhoff, S. B., Paniconi, C., Maxwell, R. M., Putti, M., and Kollet, S. J.: A comparison of two physics-based
- 880 numerical models for simulating surface water-groundwater interactions, Adv. Water Resour., 33, 456-467,
- 881 https://doi.org/10.1016/j.advwatres.2010.01.010, 2010.
- 882 Trenberth, K.: Changes in precipitation with climate change, Clim. Res., 47, 123-138, https://doi.org/10.3354/cr00953,
- 883 2011.
- 884 Valcke, S.: The OASIS3 coupler: a European climate modelling community software, Geosci. Model Dev., 6, 373–388,
- 885 https://doi.org/10.5194/gmd-6-373-2013, 2013.
- 886 Voldoire, A., Saint-Martin, D., Sénési, S., Decharme, B., Alias, A., Chevallier, M., Colin, J., Guérémy, J.-F., Michou, M.,
- 887 Moine, M.-P., Nabat, P., Roehrig, R., Salas y Mélia, D., Séférian, R., Valcke, S., Beau, I., Belamari, S., Berthet, S., Cassou,
- 888 C., Cattiaux, J., Deshayes, J., Douville, H., Ethé, C., Franchistéguy, L., Geoffroy, O., Lévy, C., Madec, G., Meurdesoif, Y.,
- 889 Msadek, R., Ribes, A., Sanchez-Gomez, E., Terray, L., and Waldman, R.: Evaluation of CMIP6 DECK Experiments With
- 890 CNRM-CM6-1, J. Adv. Model. Earth Syst., 11, 2177–2213, https://doi.org/10.1029/2019MS001683, 2019.
- 891 Williams III, J. L., Maxwell, R. M., and Monache, L. D.: Development and verification of a new wind speed forecasting
- 892 system using an ensemble Kalman filter data assimilation technique in a fully coupled hydrologic and atmospheric model, J.
- 893 Adv. Model. Earth Syst., 5, 785–800, https://doi.org/10.1002/jame.20051, 2013.
- 894 Zängl, G., Reinert, D., Rípodas, P., and Baldauf, M.: The ICON (ICOsahedral Non-hydrostatic) modelling framework of
- 895 DWD and MPI-M: Description of the non-hydrostatic dynamical core, Q. J. R. Meteorol. Soc., 141, 563–579,
- 896 https://doi.org/10.1002/qj.2378, 2015.
- 897 Zhang, L., Poll, S., and Kollet, S.: Large-eddy simulation of soil moisture heterogeneity-induced secondary circulation with
- 898 ambient winds, Q. J. R. Meteorol. Soc., 149, 404–420, https://doi.org/10.1002/qj.4413, 2023.
- 899 Zhang, L., Li, L., Zhang, Z., Arnault, J., Sobolowski, S., Chen, X., Lu, J., Mwanthi, A. M., Kad, P., Hassan, M. A., Portele,
- 900 T., Kunstmann, H., and Zuo, Z.: Enhanced hydrological modeling with the WRF-Hydro lake-reservoir module at a
- 901 convection-permitting scale: a case study of the Tana River basin in East Africa, Hydrol. Earth Syst. Sci., 29, 4109–4132,
- 902 https://doi.org/10.5194/hess-29-4109-2025, 2025.
- 903 Zhang, Y., Wagner, N., Goergen, K., and Kollet, S.: Summer evapotranspiration-cloud feedbacks in land-atmosphere
- 904 interactions over Europe, Clim. Dyn., 62, 10767–10783, https://doi.org/10.1007/s00382-024-07475-w, 2024.
- 905 Zipper, S. C., Keune, J., and Kollet, S. J.: Land use change impacts on European heat and drought: remote land-atmosphere
- 906 feedbacks mitigated locally by shallow groundwater, Environ. Res. Lett., 14, 044012,
- 907 https://doi.org/10.1088/1748-9326/ab0db3, 2019.